Transition Metal Oxides for Aqueous Sodium-Ion Electrochemical Energy Storage

Journal:	*Inorganic Chemistry Frontiers*
Manuscript ID	QI-REV-02-2018-000148.R1
Article Type:	Review Article
Date Submitted by the Author:	19-Mar-2018
Complete List of Authors:	Boyd, Shelby; North Carolina State University, Materials Science & Engineering Augustyn, Veronica; North Carolina State University, Materials Science & Engineering

Transition Metal Oxides for Aqueous Sodium-Ion Electrochemical Energy Storage

Shelby Boyd & Veronica Augustyn*

Department of Materials Science & Engineering

North Carolina State University

Raleigh, NC 27695

*vaugust@ncsu.edu

Author Biographies

Shelby Boyd is a graduate student researcher and NSF Graduate Research Fellow at North Carolina State University in the Department of Materials Science and Engineering, under the supervision of Prof. Veronica Augustyn. She received her B.S. in Materials Engineering from California Polytechnic State University in 2015. Her current research is on the synthesis and characterization of sodium ion transition metal oxides for aqueous electrochemical energy storage.

Veronica Augustyn is an Assistant Professor of Materials Science & Engineering at North Carolina State University. Her research is focused on the synthesis and characterization of materials operating at electrochemical interfaces. In particular, she is interested in the relationships between material composition, structure, and morphology and the resulting redox behavior and electrochemical mechanisms. She is the recipient of a 2017 NSF CAREER Award and a 2016 Ralph E. Powe Jr. Faculty Enhancement Award, and is a 2017 Scialog Fellow in Advanced Energy Storage from the Research Corporation for Science Advancement.

Abstract

The electrochemical storage of sodium ions from aqueous electrolytes in transition metal oxides is of interest for energy and sustainability applications. These include low-cost and safe energy storage and energy-efficient water desalination. The strong interactions between water and transition metal oxide surfaces, as well as those between water and sodium ions, dictate the stability and electrochemical energy storage mechanisms in these materials. This review summarizes the implications of water as an electrolyte solvent for transition metal oxide electrodes, and sodium ion intercalation from neutral pH electrolytes into a diverse set of transition metal oxides. Increased control of the aqueous electrolyte/transition metal oxide interface is likely to lead to improvements in stability and capacity, which are critical breakthroughs for the implementation of transition metal oxides in aqueous sodium ion energy storage technologies.

I. Introduction

A. Motivation for Aqueous Sodium-Ion Electrochemical Energy Storage

Aqueous rechargeable electrochemical energy storage based on sodium ions (Na^+) is attractive because of the potential for low cost, sustainability, high safety, and high power capability. Such devices would be of particular interest for large-scale and safety-sensitive applications, such as in renewable energy microgrids or on aircraft, as well as in emerging water desalination technologies.[1–3] Since the early 1990's, non-aqueous Li^+-based electrochemical energy storage has dominated both energy storage research and commercialization. However, recent advancements in understanding the intercalation chemistry of Na^+ in transition metal oxides and the electrochemical stability of aqueous electrolytes have rendered aqueous rechargeable Na^+ energy storage a highly active area of research, with great potential for impact in the aforementioned applications. This review focuses on the recent developments in the aqueous electrochemistry of Na^+ storage in transition metal oxides. Special attention is dedicated to reviewing the important implications of water as an electrolyte and solvent, and the electrochemical mechanisms occurring at transition metal oxide interfaces. **Figure 1** illustrates the obstacles that must be overcome and the benefits offered by aqueous rechargeable Na^+ electrochemical energy storage.

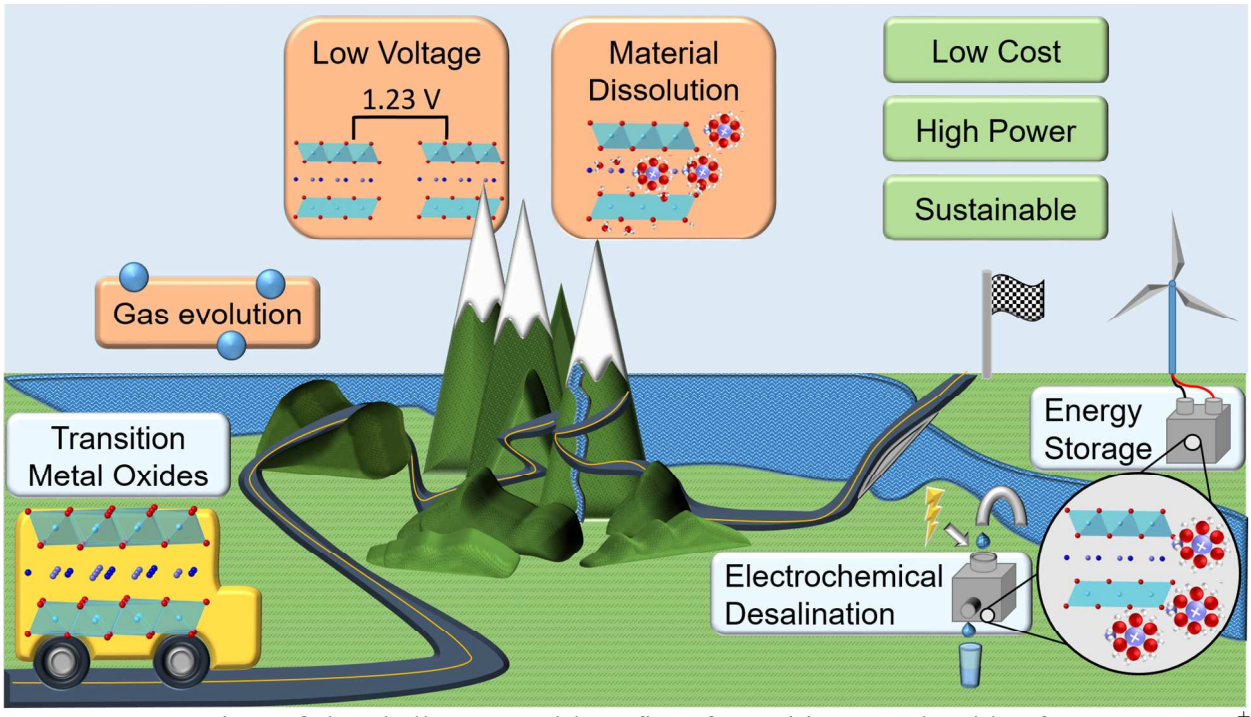

Figure 1. Overview of the challenges and benefits of transition metal oxides for aqueous Na^+ electrochemical energy storage.

B. Differences Between Aqueous and Non-Aqueous Electrochemical Energy Storage

The unique properties of water lead to many differences between aqueous and non-aqueous energy storage devices. Aqueous electrolytes offer better safety and higher power density than non-aqueous electrolytes due to the lack of flammable solvents and the higher ionic conductivity of inorganic salts in aqueous solutions. Typical conductivities of aqueous electrolytes are between 10 - 190 mS cm^{-1},[4] while those of non-aqueous electrolytes are < 10 mS cm^{-1}.[5] The power densities of commercialized rechargeable batteries are limited by the ionic conductivities of the electrode materials. However, with the advent of nanostructured electrode materials with high power densities,[6] there will be an increased need for higher conductivity electrolytes such as

aqueous solutions. With increased power density, particularly in safety-sensitive applications, the importance of using non-flammable electrolytes is also likely to increase.

Negative attributes of aqueous electrolytes in energy storage devices are that they provide a smaller potential window of stability (1.23 V) and lead to the development of a highly structured electrolyte at the electrochemical interface,[7–9] and that they can exhibit corrosive behavior.[10,11] These all lead to degradation of both the active electrode materials and auxiliary components such as current collectors.[4,10] In non-aqueous batteries, degradation of the electrolyte at the electrochemical interface can lead to a stable, ionically conductive, and electronically insulating layer termed the cathode-electrolyte interface (CEI), or the solid-electrolyte interface (SEI) at the anode.[12,13] These degradation layers are hypothesized to stabilize the electrochemical interface upon further cycling, minimizing the occurrence of parasitic reactions at the electrode-electrolyte interface. However, an analogous SEI or CEI formation process does not occur in standard low-to-moderate concentration aqueous electrolytes, because the degradation byproducts of water are either volatile gases (H_2, O_2), or reactive ions (H^+, OH^-), none of which will form a solid deposit.[14,15] As conceptualized in **Figure 2,** the surface vulnerability of electrodes in aqueous electrolytes is one of the key differences between aqueous and non-aqueous energy storage. This vulnerability leaves the electrode surface in aqueous electrolytes open to dissolution and available to catalyze the decomposition of the electrolyte, which lead to decreased electrochemical stability and therefore low cyclability. As a result, there are significant efforts underway to understand and control the fundamental mechanisms occurring at aqueous electrolyte/transition metal oxide interfaces during electrochemical energy storage.

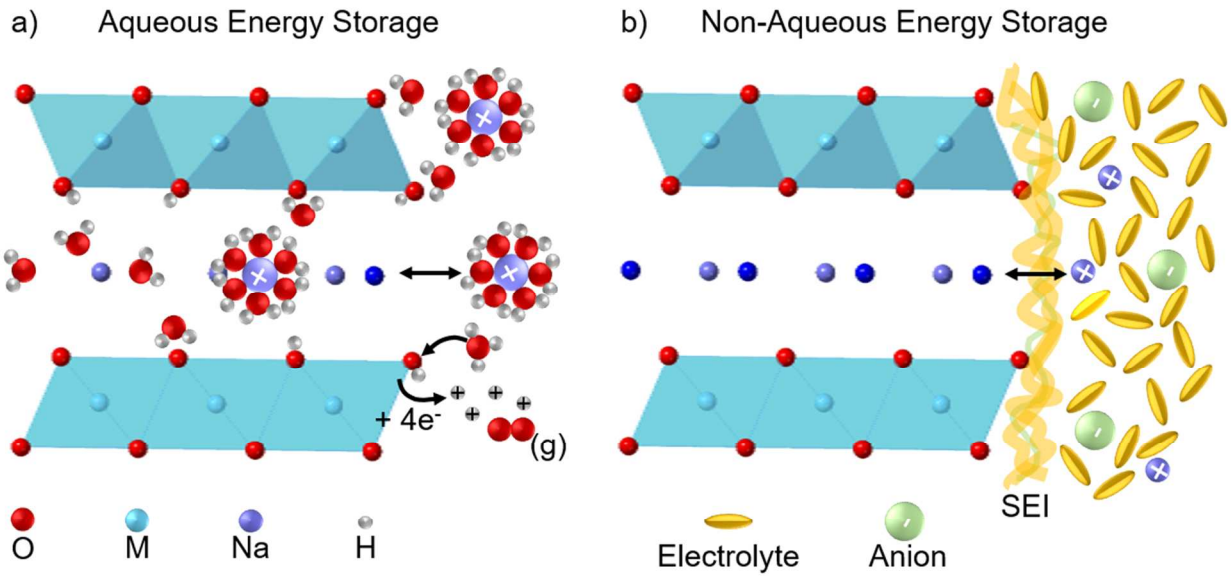

Figure 2. a) Transition metal oxides interact strongly with aqueous electrolytes. This includes the coordination of the surface by water molecules and possibility of catalyzing the oxygen evolution and hydrogen evolution reactions and co-intercalation of cations with water molecules into the structure, b) Transition metal oxides in non-aqueous electrolytes are often protected from solvent co-intercalation and repeated electron transfer to the electrolyte by the formation of an electrolyte decomposition layer during the first few cycles.

II. Water as an Electrolyte Solvent

A. Unique Aspects of Water as an Electrolyte Solvent

Water is a unique solvent and electrolyte because of its small molecular size and high polarity.[9] These properties increase the solubility of electrolyte salts, as the small size allows multiple water molecules to interact with ions, and the high polarity allows for bonding between water and cations.[16] This polarity also leads to a secondarily-bonded electrolyte structure, and

much stronger electrode-electrolyte interactions at the transition metal oxide surface than those in non-aqueous electrolytes.[9] Because water autodissociates into OH^- and H_3O^+, it contains ions that can readily react with surfaces and are generally corrosive. This can be addressed, but requires special care in material choice and device design. The small size of water coupled with the high hydration energy of inorganic cations also allows it to readily co-intercalate into many transition metal oxides.[17]

B. Structure of Water at the Electrode-Electrolyte Interface

Within the bulk liquid, water tends to form short-range ordered networks of tetrahedrally hydrogen-bonded water molecules.[18] Because of these hydrogen-bonded water molecule networks, water can be considered as an oxide held together by hydrogen bonds.[9,19] Within the electrolyte, solvated metal cations are fully coordinated by water molecules, and a metal-oxygen bond forms between the cation and the lone pairs on the oxygen atoms of water molecules within the inner coordination solvation sphere. On the other hand, most simple anions substitute for water molecules in the hydrogen-bonded network due to their negative charge and similar size to O^{2-}, and interact with water molecules via hydrogen bonding.[18] The electrolyte in the bulk and at the interface is dynamic: a high frequency of bond formation and rupture occurs between water molecules, dissolved ions, and the electrode surface.

The interactions of water with oxide surfaces are complex, and fundamental to understanding a wide array of chemical mechanisms, from energy storage to geological weathering. The pristine surfaces of oxides expose under-coordinated metal cations and oxygens. The metal surface sites act as Lewis acids while the oxygen surface sites as Lewis bases. The bonding and arrangement of water with oxide surfaces is in large part driven by acid-base

interactions between the surface and the water. Water is an ampholyte, and when water molecules interact with oxide surfaces they will readily react with the under-coordinated surface sites.[20] In some oxides, these steps are only the start of hydrolysis reactions that eventually lead to the formation of new hydroxide phases on the surface.[21] Once formed, these hydrated surfaces and nearby water do not remain static. Several well-known, albeit static, models have been used to describe the general organization of aqueous electrolytes at an electrode surface. Most build off the limiting cases of the simple Gouy-Chapman-Stern model (**Figure 3a**).[7] In this model, the Inner Helmholtz Plane is composed of adsorbed water molecules, while the Outer Helmholtz Plane consists of hydrated cations. These two planes form a parallel-plate capacitor, the width of which is called the Stern layer.[8] The Stern layer has been shown to narrow with increasing salt concentration, which can increase the electrical double-layer capacitance at the interface.[8]

C. Stability of Aqueous Electrolytes

When water interacts with an electrochemical interface at a potential below that of the hydrogen evolution reaction (HER), or above that of the oxygen evolution reaction (OER), electrons are transferred between the electrode and electrolyte. The thermodynamic stability window of water spans 1.23 V, and the potentials at which the HER and OER occur vary with pH, as shown in the Pourbaix diagram of water (**Figure 3b**). The reaction products produced from these reactions can alter the local pH at the oxide-electrolyte interface and greatly affect oxide stability.[22–24] In addition, these reactions are not isolated to oxide materials and should be taken into consideration for other electrode material systems.

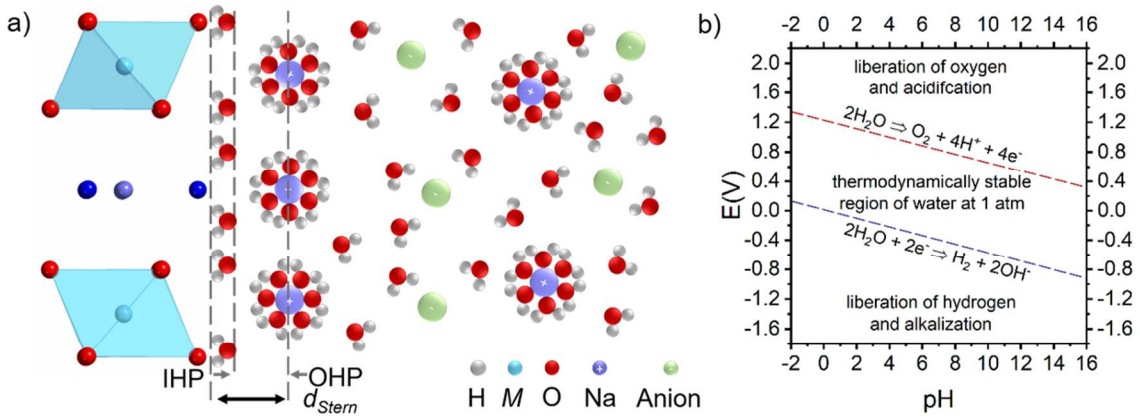

Figure 3. a) Gouy-Chapman-Stern model of the electric double layer at a transition metal oxide/aqueous electrolyte interface. The electrochemical potential at the electrode-electrolyte interface decreases linearly across the Stern layer thickness (d_{Stern}), where the coordinated waters of the Inner Helmholtz Plane (IHP) and hydrated cations of the Outer Helmholtz Plane (OHP) form a structured layer of water at the interface, b) The potential-pH, or Pourbaix, diagram of water, showing stability region of water as between the OER (upper dashed line) and HER (lower dashed line) (adapted from Ref. 25).

D. Overcoming Stability Limitations

Approaches to improving the stability of oxides (as well as other electrode materials) in aqueous Na^+ electrolytes include: (1) removing dissolved oxygen,[26–28] (2) introducing an electrolyte additive or electrode surface coating that conducts ions but prevents water molecules from contacting the active material,[24,27,29,30] and (3) using a high concentration electrolyte to decrease the number of free water molecules available to participate in side reactions.[4,14,28,31–33] All of the electrolyte-based approaches to improving stability endeavor to remove the driving force for water molecules to undergo decomposition reactions at the electrode surface.

a. Removal of Dissolved O_2 From the Electrolyte

A common practice when working with aqueous electrolytes is to remove dissolved O_2 (and CO_2) from the electrolyte by bubbling N_2 and Ar into the cell before electrochemical characterization.[26–28,34–36] After deaerating the electrolyte, most studies demonstrate mild improvements in the short-term cycling stability and Coulombic efficiency.[4,26,34] However, long term cycling results show a severe drop in performance, indicating that removal of excess oxygen from the electrolytes does not completely address the challenges of electrochemical energy storage in aqueous electrolytes.[34,36]

b. Electrolyte Additives

Another method of expanding the stability window of aqueous electrolytes is to add surfactants that form, ideally, an ionically conductive protective layer on the electrode surface.[24,27] One report on aqueous lithium-ion batteries found that a 0.25 M Li-PO_4 buffer solution saturated with disodium propane-1,3-disulfonate (PDSS) exhibited better anodic stability than $LiNO_3$ electrolytes, with the OER suppressed up to 1.6 V *vs*. Ag/AgCl.[24] While a surface film was not found when the electrode was removed from the electrolyte, there was a significant decrease in the current density ascribed to the OER. This suggested that the bulky PDSS anion acted as a barrier between water molecules in the electrolyte and the electrode surface. The report by Hou *et al.* supported the concept that surfactants, including sodium dodecyl sulfate, can inhibit the HER and OER when added to aqueous electrolytes at or above their critical micelle concentration.[27] In a 1 M sodium sulfate (Na_2SO_4) and zinc sulfate ($ZnSO_4$) electrolyte with sodium dodecyl sulfate added at the critical micelle concentration, the potential window was expanded from 1.8 to 2.55 V (**Figure 4a**). Capacity retention of the energy storage device also improved with the surfactant-containing aqueous electrolyte, from 13% to 95% after

200 cycles at 0.5C (**Figure 4b**). The C-rate is used to designate the rate at which a battery is charged or discharged; C represents the maximum or theoretical capacity, divided by the charge or discharge time in hours. These electrolyte additives allow higher cyclability than deaerated electrolytes, and offer a cheaper alternative to the water-in-salt electrolytes described below, although they do not reach as high of anodic potentials.

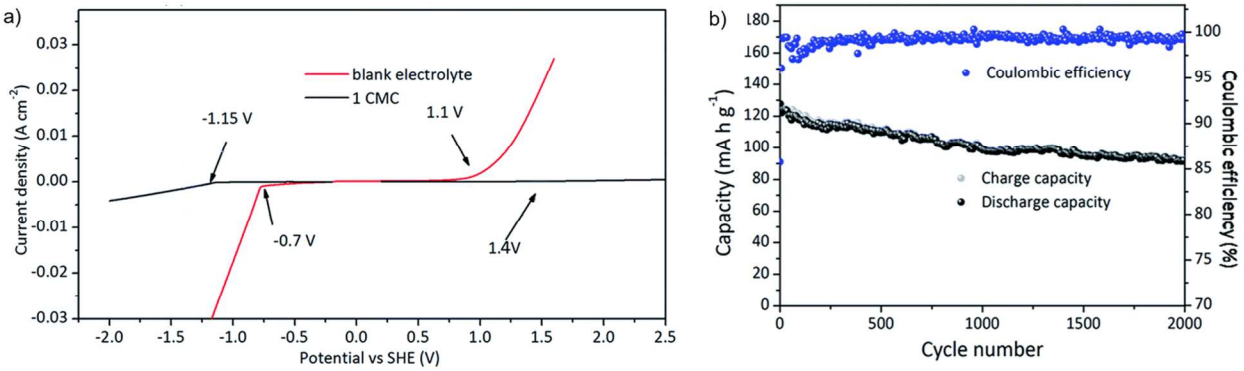

Figure 4. Effect of aqueous electrolyte additives on the electrochemical potential window and energy storage device lifetime. a) Linear sweep voltammetry at 10 mV s^{-1} on titanium mesh of a 1 M Na_2SO_4 and $ZnSO_4$ electrolyte with ("1 CMC") and without ("blank electrolyte") sodium dodecyl sulfate, b) Cyclability of a Prussian blue analog/Zn cell in 1 M Na_2SO_4 and $ZnSO_4$ electrolyte with sodium dodecyl sulfate at 5C. Adapted with permission from Ref. 27. Copyright 2017 Royal Society of Chemistry.

c. High Electrolyte Concentration

The most successful approach to date to widen the potential window of aqueous electrolytes has been to utilize highly concentrated and water-in-salt electrolytes. This approach has been applied successfully in Li^+, Na^+, Mg^{2+}, and Zn^{2+} aqueous electrolytes.[10,14,15,30–33,37] The

stability window of aqueous electrolytes has been expanded to 2.6 V in Na^+ and 3.1 V in Li^+ water-in-salt electrolytes (WiSE) made with ultrasoluble salts.[30,32] High salt concentrations disrupt the hydrogen bonded water network, decreasing overall electrolyte conductivity as the number of interactions between the water molecules and electrolyte salts increase and the number of both free water molecules and water molecules coordinated to each salt ion decrease.[38] In these electrolytes, ions often exist as contact ion pairs (CIP) or cation-anion aggregates in addition to the solvent-separated ion pairs (SSIP) present in traditional salt-in-water electrolytes (SiWEs).[14,31,32] Cation mobility in WiSEs remains high due to their unique coordination in aqueous electrolytes, where a significant fraction of cations remain as higher mobility hydrates and SSIPs, and the anions form a network of CIPs and ion aggregates.[31,39] Most importantly, this approach reduces or eliminates free water molecules available to approach the electrode surface.

There are two strategies for the use of high concentration aqueous electrolytes. The first is to increase the electrolyte salt concentration but keep water as the majority component, resulting in a high-concentration SiWE.[31] In studies of electrochemical double layer capacitors, the use of a concentrated 5 M $NaClO_4$ aqueous electrolyte significantly increased both the capacitance and power density due to increased ionic conductivity and decreased hydration of the Na^+.[32,38] With a higher salt concentration in the electrolyte, each Na^+ was coordinated by fewer water molecules and was able to pack more closely into the pores of the carbon electrode.[38] At concentrations higher than 5 M, the ionic conductivity of the electrolyte began to decrease.[4] The effect of concentration on cycling stability of a full cell with $NaTi_2(PO_4)_3$ as the anode and $Na_{0.44}MnO_2$ as the cathode was studied with aqueous electrolyte concentrations of 0.1, 1, and 5 M $NaClO_4$ between 0.6 - 1.4 V.[4] The capacity, reversibility, self-discharge time, polarization, and rate

capability of the cell all improved with increased electrolyte concentration. Although the improved performance was attributed to the lower content of dissolved oxygen in higher concentration electrolytes, the reduced activity of water and number of free water molecules also likely contributed to the cell stability. Despite these improvements, high concentration SiWE are unlikely electrolytes for high-voltage aqueous energy storage due to the marginal improvements in capacity loss and potential window as compared to more dilute aqueous electrolytes.

WiSEs are made with ultrasoluble salts, and contain more salt than water by both weight and volume.[14] They provide a low reactivity and high cycling stability due to the exclusion of water from the electrode-electrolyte interface at anodic potentials,[40] and the formation of a protective layer at the electrode surface analogous to the non-aqueous SEI/CEI.[14] The first example of a WiSE system was shown in 2015 by Suo et al., with a 21 m lithium bis(trifluorosulfonyl)imide (LiTFSI) WiSE.[14] The reduction potential of $TFSI^-$ anion is above that of water, allowing the formation of an SEI-like anode/electrolyte interface due to the reduction of the anion. The combination of reduced water activity at a high electrolyte concentration and the formation of an interphase layer on the anode allowed for a high 3 V potential window of the WiSE, and a cell voltage of 2.3 V. Follow-up studies achieved a cell voltage of 2.5 V either by using a 28 m LiTFSI-LiOTF bisalt electrolyte,[30] or by adding 0.1 wt % tris(trimethylsilyl) borate to the 21 m LiTFSI WiSE to form a protective CEI.[15] A 4.2 V electrolyte stability window was reported on an Al foil current collector in 21 m LiTFSI.[10]

The report on Li^+ systems was followed by the successful application of the WiSE concept to an aqueous Na^+ battery based on $NaTi_2(PO_4)_3$ as the anode and $Na_{0.66}Mn_{0.66}Ti_{0.34}O_2$ as the cathode, with 9.21 M sodium trifluoromethane sulfonate (NaOTF) as the electrolyte.[31] This electrolyte exhibited an electrochemical stability window of 2.5 V, and the full electrochemical

cell voltage was 1.4 V (**Figure 5a**). This cell exhibited some HER activity (**Figure 5b**), but only experienced 0.006 % capacity loss per cycle for 1,200 cycles at 1C (**Figure 5c**). Even at a relatively low concentration of ~ 9 m, theory and spectroscopic evidence indicate that the Na^+ ion is coordinated by both the F and O atoms of the OTF^- anion, with ~ 30 % of ions existing as SSIPs. When these ion pairs are reduced at the anode, they form an Na^+-conducting SEI-like layer.[31] Both WiSE and SiWE composed of NaOTF form SEIs at the anode after ~1,000 cycles, but the WiSE SEI better shielded the electrode from electron tunneling, as evidenced by the slower voltage decay of WiSE cells during self-discharge measurements.

Recent work by Kühnel, Reber, and Battaglia found that sodium bis(fluorosulfonyl)imide (NaFSI) is soluble up to 37 m in water, and when used in a WiSE it can double the stable potential window of water from 1.23 V to 2.6 V.[32] Raman spectroscopy of LiTFSI and NaFSI WiSE showed that the local water molecule environment in 35 m NaFSI electrolyte is like that of the 21 m LiTFSI electrolyte. Cycling stability remains to be studied in this system. Overall, WiSE systems allow for the highest voltage aqueous energy storage devices to date. Moreover, the unique properties of water allow unexpectedly high cation conductivities in these more viscous, high salt concentration electrolytes.[31,39] The high Na^+ conductivity, cycling stability, and cell voltage of the WiSE systems make this one of the most promising research directions for aqueous Na^+ energy storage.

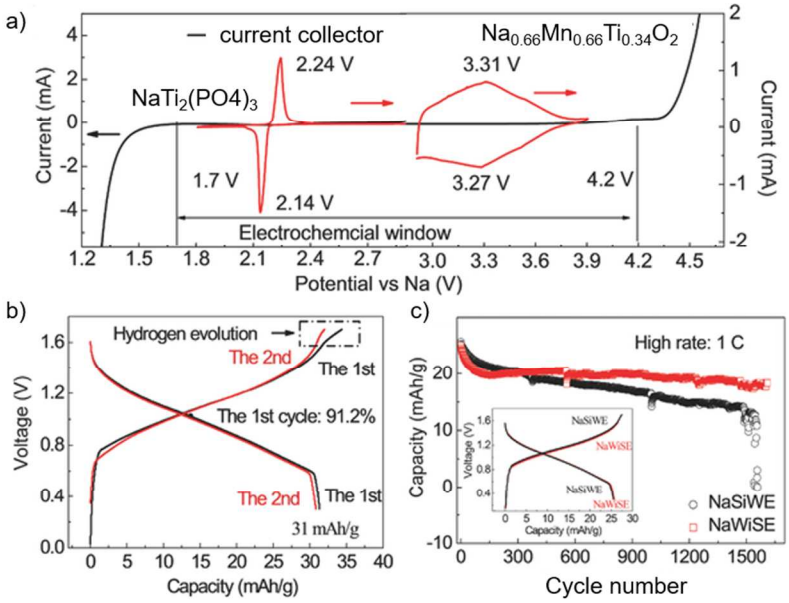

Figure 5. Effect of aqueous electrolyte concentration on the electrochemical potential window and energy storage device lifetime. a) The 2.5 V electrochemical potential window of a 9 m NaOTF WiSE, b) Galvanostatic cycling of an electrochemical cell made with the 9 m NaOTF WiSE with $NaTi_2(PO_4)_3$ as the anode and $Na_{0.66}Mn_{0.66}Ti_{0.34}O_2$ as the cathode, and c) Cycling stability of the NaOTF WiSE cell as compared to a 2 m NaOTF SiWE. Adapted with permission from Ref. 31. Copyright 2017 John Wiley and Sons.

E. Experimental Considerations

Due to the corrosive nature of aqueous electrolytes, it is important that all cell components are electrochemically stable. This can lead to tradeoffs in performance. For example, while chloride salts have a higher ionic conductivity than sulfate salts, they are more corrosive towards stainless steel, so many studies on aqueous Na^+ energy storage use Na_2SO_4 as the electrolyte salt.[11] A recent investigation of aqueous Na^+ batteries for wearable applications compared the

performance of batteries with stainless steel mesh or carbon nanotube (CNT) current collectors in three different electrolytes: 1 M Na_2SO_4, 0.9 M NaCl, and cell culture saline solution.[34] It was found that the stainless steel current collectors were more electrochemically stable than the CNT current collectors, which required deoxygenation before cycling. Besides stainless steel, other candidates for current collectors in neutral pH aqueous electrolytes are titanium mesh[27] and graphite foil.[41] Aluminum foil may also be viable when used in conjunction with a WiSE, highlighting the possibility of using a cheaper and less dense material than the most common titanium and stainless steel current collectors.[10]

III. Transition Metal Oxides for Aqueous Sodium-Ion Electrochemical Energy Storage

Transition metal oxides are of interest for aqueous Na^+ energy storage due to their high gravimetric capacity, stability in ambient atmosphere, and tunability of redox potentials depending on composition.[35,42–52] As will be discussed in the following sections, major challenges for this class of materials in Na^+ aqueous electrolytes include dissolution, side reactions with the electrolyte, and low electronic conductivity.[25,50–57] Other materials studied for aqueous Na^+ energy storage include Prussian blue analogues, polyanionic phosphates, and organic materials. Prussian blue analogues can be used for electrochemical desalination and as cathodes for aqueous Na^+ energy storage.[3,58] They have an open framework structure, which leads to large ion intercalation sites suitable for Na^+ storage with good power capability and cycling stability in aqueous electrolytes.[1,59–61] Disadvantages of Prussian blue analogues include their low theoretical capacity (~ 60 mAh g^{-1}) and de-sodiated as-synthesized state.[61,62] Polyanionic structures, such as olivine $NaFePO_4$, $NaFeP_2O_7$, and Na^+ superconductor (NASICON) type $NaTi_2(PO_4)_3$ and $Na_3V_2(PO_4)_3$, are commonly studied as anode materials for

aqueous Na^+ energy storage.[1,4,22,28,31,60,63–68] The main drawbacks of phosphate materials in aqueous electrolytes are their significant capacity fade during cycling, low ~ 40 - 60 mAh g^{-1} capacity, and low electronic conductivity.[1,22,60,63,66] Finally, the nascent studies of organic electrode materials offer promising results, although much remains to be studied in these systems. Materials such as polyimides have shown stability and capacity competitive with transition metal oxides for aqueous Na^+ anodes.[69] Recent review papers discuss these non-oxide materials in greater detail.[1,60,69] Thus far, transition metal oxides remain the most widely studied electrode materials for aqueous Na^+ energy storage.

A. Binary Transition Metal Oxides

a. Manganese Dioxide (MnO_2)

Of the several polymorphs of MnO_2, amorphous MnO_2, λ-MnO_2 (spinel), α-MnO_2 (hollandite), and δ-MnO_2 (birnessite) are the most studied for Na^+ storage in aqueous electrolytes. It has been reported that the tunnel-structured α-MnO_2 and layered δ-MnO_2 phases, shown in **Figure 6a**, have large enough intercalation sites (at least ~ 4.6 Å) for significant Na^+ storage.[49] Oxidation of the spinel in aqueous electrolytes containing cations other than Li^+ (such as Na^+) drives a phase transformation to δ-MnO_2 as water is chemically intercalated to compensate for electrons and cations lost during oxidation.[70,71] The other phases, including amorphous MnO_2, show intercalation of protons (H^+) and high surface storage of H^+ and Na^+ via pseudocapacitance.[46–49] It should be noted that while often identified as "MnO_2," Mn atoms in δ-MnO_2 and α-MnO_2 exist in mixed valence states and additional cations (e.g. Na^+, K^+, Mg^{2+}) and

structural water molecules are incorporated during synthesis to balance charge and stabilize the structure.[46,49,72,73]

Two types of electrochemical energy storage mechanisms have been found for MnO_2 in aqueous electrolytes: surface-based pseudocapacitance and intercalation into the bulk material.[48,49,74,75] Both follow the same redox process:

$$MnO_2 + xA^+ + xe^- \leftrightarrow A_xMnO_2 \quad (1)$$

where A^+ can be a proton or an alkali metal cation. This reaction is generally active between 0 and 1 V (*vs*. a saturated calomel electrode, SCE) in neutral pH aqueous electrolytes. Pseudocapacitive energy storage in MnO_2 in aqueous electrolytes leads to exceptional capacity retention.[76] However, most MnO_2 phases that experience Na^+ intercalation into the bulk see capacity deterioration within several hundred cycles. This can be explained with the Pourbaix diagram of MnO_2 in water (**Figure 6b**), which shows that, within the potential range of aqueous electrolytes and at acidic and neutral pH, the stable species is soluble Mn^{2+}. MnO_2 experiences reductive dissolution. Upon protonation to MnOOH at the surface, it can spontaneously disproportionate and form soluble Mn^{2+}:[77,78]

$$2Mn^{3+} \rightarrow Mn^{2+} + Mn^{4+} \quad (2)$$

Electrochemical reduction of MnO_2 has led to dissolution of the manganese at ~ -0.1 V *vs*. Ag/AgCl in aqueous and non-aqueous electrolytes.[53]

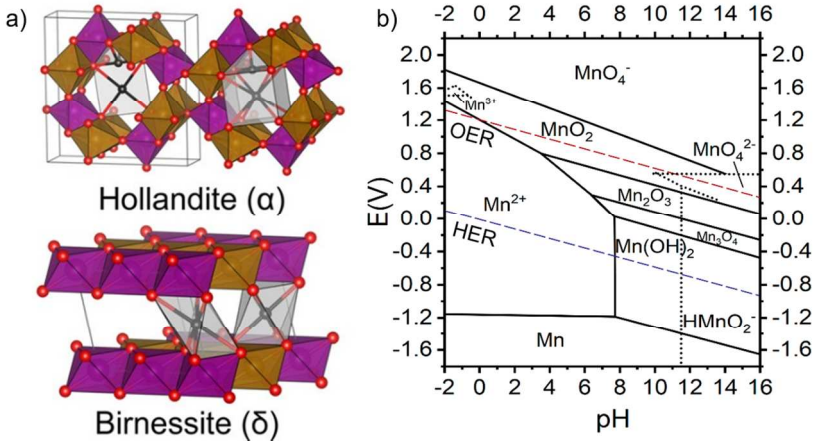

Figure 6. a) The crystal structures of α-MnO_2 and δ-MnO_2, two polymorphs of MnO_2 that are capable of bulk intercalation of Na^+; the Na^+ intercalation sites are indicated by the gray polyhedra. Adapted with permission from Ref. 46. Copyright 2017 American Chemical Society. b) The Pourbaix diagram of MnO_2 in water (adapted from Ref. 25).

i. Amorphous MnO_2

Amorphous MnO_2 exhibits pseudocapacitive behavior in neutral pH aqueous electrolytes, as first reported by Lee and Goodenough.[79] This study utilized three chloride electrolytes: 2 M KCl, NaCl, and LiCl. Of these, the fastest kinetics were observed with KCl, which was attributed to the smaller charge density and hydration shell of K^+ as compared to Na^+ and Li^+. In Na^+-containing electrolytes, amorphous MnO_2 has shown a capacitance of 253 F g^{-1} (84 mAh g^{-1}) between - 0.2 – 1 V *vs*. SCE at 0.5 mV s^{-1}, with a capacity retention of 44 % after 1,000 cycles.[48] A hybrid electrochemical device consisting of pseudocapacitive, mesoporous MnO_2 and activated carbon (which provided only double layer capacitance) had a capacitance of 80 F g^{-1}

(37.3 mAh g^{-1}) and maintained ~ 98 % capacity after 5,000 cycles.[76] The pseudocapacitive behavior of amorphous MnO_2 is indicated by highly reversible electrochemical behavior: rectangular cyclic voltammograms, fast switching times, and surface/interface limited redox kinetics.[80]

ii. Hollandite α-MnO_2

The α-MnO_2 structure (**Figure 6a**) consists of small 1 x 1 tunnels, and larger 2 x 2 (~ 4.6 Å) tunnels capable of accommodating reversible cation intercalation.[49] In addition to its potential as a Na^+ energy storage material, α-MnO_2 has been studied as a redox-active material for electrochemical desalination.[81] This phase can be crystalized from amorphous MnO_2 at ~ 300 - 400 ºC.[48,76] Electrochemistry of α-MnO_2 in 0.1 M Na_2SO_4 shows that capacitance greatly depends on surface area, with values ranging from 50 F g^{-1} (16 mAh g^{-1}) between -0.2 - 1.0 V *vs*. SCE at 0.5 mA cm^{-2}, to 240 F g^{-1} (67 mA h g^{-1}) between 0 - 1.0 V *vs*. SCE at 20 mV s^{-1}.[48,49] This material is of interest for electrochemical capacitors due to its high rate capability,[51] and exhibits a moderate capacity retention of 75% after 100 cycles at 0.5 mA cm^{-2}.[49] The loss in capacity retention is likely due to dissolution of manganese in the aqueous electrolyte.

iii. Birnessite δ-MnO_2

The pseudocapacitive properties and electrochemical stability of δ-MnO_2 are in large part due to the presence of interlayer structural water.[35,42,43] The δ-MnO_2 structure is monoclinic[11] for monohydrates with interlayer alkali metal ions (e.g. $Na_xMnO_2{\cdot}nH_2O$), and hexagonal for monohydrates with interlayer transition metals or dihydrates with alkali and transition metals.[82]

According to the Delmas notation, δ-MnO_2 is a layered oxide with an O3 stacking sequence.[83] The layers consist of edge-sharing MnO_6 octahedra separated by inter-lamellar structural water molecules and metal cations (Figure 6a).[11,70] Refinement of the (004) peak in XRD patterns shows that water occupies Na^+ sites within the interlayer.[35] It can be synthesized by a hydrothermal reaction of an alkali metal permanganate precursor in acid or by electrochemical cycling of λ-MnO_2, $Mn(OH)_2$, or $NaMnO_2$ in aqueous electrolytes.[42,70,71,82,84]

Studies of δ-MnO_2 in both aqueous and non-aqueous electrolytes show that the presence of interlayer structural water increases the interlayer distance from ~ 5 to 7 Å, leading to an increase in Na^+ diffusion, capacity, rate capability, and cycle life, while decreasing interfacial charge transfer resistance.[35,42,43] The interlayer water remains stable in the structure during cycling, and is hypothesized to have two major benefits. First, interlayer water partially hydrates Na^+ within the layer and replaces electrolyte water molecules in the hydration shell of intercalating Na^+, reducing the electrolyte-electrode interfacial resistance and providing electrostatic shielding within the material that decreases its diffusion resistance.[35,42] Second, the structural water molecules act as pillars and reduce internal stresses, preserving the layered structure during cycling and decreasing the dissolution of Mn^{2+} in the electrolyte.[35,42,43]

δ-MnO_2 can be synthesized with cations other than Na^+, most commonly K^+ or Mg^{2+}. Synthesizing the δ-MnO_2 with cations other than Na^+ increases the interlayer spacing and improves the capacity and rate capability for Na^+ intercalation.[11,75,85] However, both Mg^{2+} and K^+ are susceptible to ion exchange with Na^+ from the electrolyte upon exposure to, and during cycling in, an aqueous Na^+ electrolyte.[11,85,86] The alkali cation ratio of δ-MnO_2 can be tuned to increase capacity, as shown in **Table I.**[75,85,87] For example, sodium-only or potassium-only δ-

MnO_2 show capacities of ~ 80 mAh g^{-1} while a dual sodium- and potassium-containing δ-MnO_2 had a capacity of ~ 134 mAh g^{-1}.[75,87]

Figure 7 compares the capacity and cycling stability of a series of $K_xNa_yMnO_2$ with varying Na : K ratios in a 1 M Na_2SO_4 aqueous electrolyte. The 2.5 Na : K material exhibited the highest capacity at 1.5C and maintained excellent capacity and rate capability, with ~60 mAh g^{-1} and over 10,000 cycles at 50C.[75] The improvement was hypothesized to be due to the ability of K^+ to act as a supporting pillar between MnO_2 layers, increasing the interlayer spacing and decreasing electrostatic attraction of Na^+ within the interlayer.[75] The decrease in capacity when all K^+ was replaced by Na^+ (Na : K = 11 : 0) was attributed to the smaller interlayer spacing of the obtained δ-MnO_2. Overall, δ-MnO_2 show a high capacity of up to ~ 134 mAh g^{-1},[75] considerable pseudocapacitive current contributions,[85] high rate capability,[75] and high electrochemical stability with up to 1,000 cycles with minimal Mn^{2+} dissolution.[11,35] Due to the abundance and safety of manganese, addressing the issue of Mn^{2+} dissolution and tuning the composition of δ-MnO_2 to increase capacity are both of interest for aqueous Na^+ energy storage.

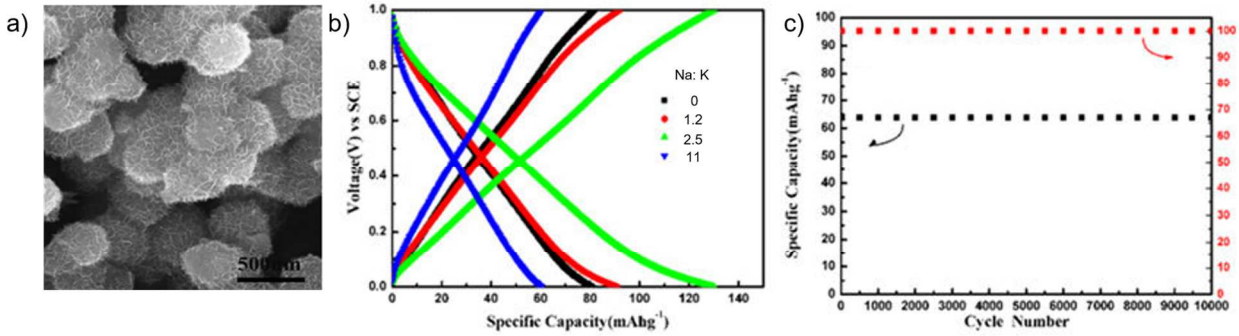

Figure 7. Scanning electron micrograph of the flower-like morphology of as-synthesized δ-MnO_2, b) Galvanostatic cycling of δ-MnO_2 with varying ratios of Na : K at 1.5C in 1 M Na_2SO_4,

and c) Cycling stability of the 2.5 Na : K material at 50C in 1 M Na_2SO_4 . Reproduced from Ref. 75. Licensed under Creative Commons CC BY.

Table I. Electrochemical performance of various δ-MnO_2 compositions in aqueous Na^+-electrolytes.

Material	Capacity (mAh g^{-1})	Capacity Retention	Ref.
$Na_{0.25}Mg_{0.07}H_{0.18}MnO_2 \cdot 0.8H_2O$	36	~ 100% (50 cycles at 2 mV s^{-1})	11
$Na_{0.58}MnO_2 \cdot 0.5H_2O$	80 (1C)	100% (150 cycles at 1C)	35
$Na_{0.58}MnO_2$	79 (1C)	60% (150 cycles at 1C)	35
$K_xNa_yMnO_2$ (x : y = 2 : 5)	134 (1.5C)	~ 100% (150 cycles at 1.5C)	75
K_xMnO_2	80 (1.5C)	~ 100% (150 cycles at 1.5C)	75

b. Molybdenum Trioxide

Molybdenum trioxide (MoO_3) is a versatile intercalation oxide, with the ability to intercalate alkali cations as well as Mg^{2+} and organic molecules.[88] The thermodynamically stable form of MoO_3 is the orthorhombic (α-MoO_3) phase, which consists of bilayers of edge- and corner-sharing MoO_6 octahedra (**Figure 8a**).[45,89] The theoretical capacity of MoO_3 is 372 mAh g^{-1} for a 2-electron redox. This oxide is redox-active below 0 V *vs*. SCE, making it useful as an anode for aqueous Na^+ energy storage.[55] The intercalation reaction with Na^+ yields a sodium bronze, Na_xMoO_3:

$$MoO_3 + xe^- + xNa^+ \leftrightarrow Na_xMoO_3 \quad (3)$$

where the maximum extent of intercalation, x, is ~ 1.5 – 2.[44,45] In aqueous electrolytes, the potential window limits the capacity to fewer than 2 electrons per MoO_3.

The intercalation electrochemistry of MoO_3 can be modified by tuning the oxygen vacancy content or the chemistry and structure of the interlayer. MoO_3 is a semiconductor, but reduction to MoO_{3-x} leads to an increase in electronic conductivity, which has been shown to enable high power capability.[44,45,56,90,91] While bulk α-MoO_3 exhibits battery-type kinetics for energy storage, nanostructured MoO_3 integrated into advanced electrode architectures demonstrates pseudocapacitive kinetics.[50,51] The kinetics of energy storage of MoO_3 can also be improved by tuning its interlayer structure and chemistry. One strategy is to increase the interlayer spacing, as was performed for hydrothermally synthesized, reduced, and potassiated K_yMoO_{3-x}.[56] It was found that aqueous electrolytes containing Na^+, K^+, and Mg^{2+} could intercalate into K_yMoO_{3-x}, achieving 196 F g^{-1} (44 mAh g^{-1}) at 0.5 A g^{-1}, with 89% capacity retention after 10,000 cycles at 1 A g^{-1}.[56]

The Pourbaix diagram of MoO_3 (**Figure 8b**) indicates that MoO_3 dissolves into molybdate anions (MoO_4^{2-}) in neutral pH aqueous solutions. While it exhibits some stability at anodic potentials and low pH, MoO_3 is not the thermodynamically stable form in the potential region in which it is redox active.[25] This is verified by experiments, which show that aqueous electrolyte-based energy storage devices with MoO_3 electrodes exhibit short lifetimes.[50,54–56] One way to address this issue is by protecting the MoO_3 from the aqueous electrolyte with a thin coating. A full aqueous Na^+ energy storage cell with polypyrrole-coated MoO_3 as the anode retained 78 % of the 33 mAh g^{-1} capacity after 1,000 cycles, while a cell with an uncoated MoO_3 anode retained < 30 % of the capacity after 50 cycles.[55] The lower capacity retention of the uncoated MoO_3 is likely due to its increased dissolution in the aqueous electrolyte. The polypyrrole coating was hypothesized to enhance cycling stability by minimizing water contact with the MoO_3, as well as by mitigating the intercalation-induced volume changes of MoO_3.[55] While

MoO_3 appears less promising than δ-MnO_2 from a capacity and conductivity standpoint, its long cycling life under the right conditions and theoretical multi-electron redox give it some potential for use as an anode in wider potential aqueous Na^+ energy storage, perhaps in devices with a WiSE.

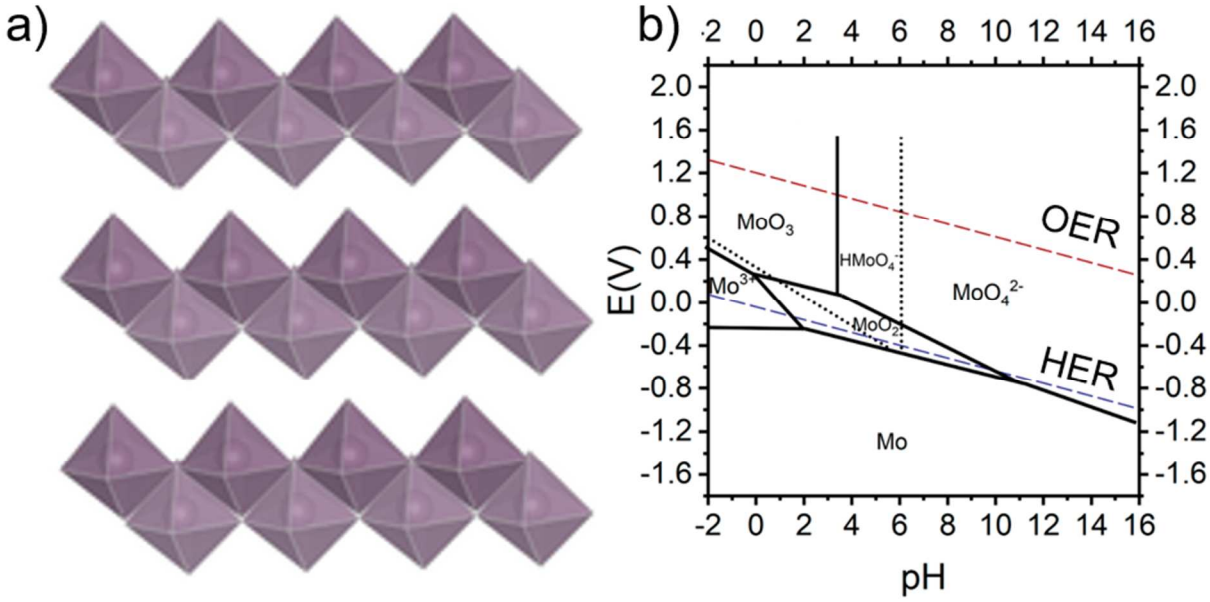

Figure 8. MoO_3 structure and solubility. a) Structure of α-MoO_3. Reproduced with permission from Ref. 92. Copyright 2017 John Wiley and Sons. **b)** Pourbaix diagram of MoO_3 in water: MoO_3 is thermodynamically stable at positive potentials and low pH electrolytes (adapted from Ref. 25).

c. Vanadium Pentoxide

Vanadium pentoxide (V_2O_5) forms a variety of layered structures which can reversibly intercalate alkali cations, including Na^+,[93–95] with a high theoretical capacity of ~ 235 mAh g^{-1} for the 2-electron redox.[52] In addition to its surface pseudocapacitive behavior, V_2O_5 intercalates

alkali cations such as Na^+ at negative potentials *vs*. SCE according to the following reaction:[52,55,94]

$$V_2O_5 + xe^- + xA^+ \leftrightarrow A_xV_2O_5 \quad (4)$$

Due to the low potential at which cation intercalation occurs, V_2O_5 and related oxides are potential anode materials for aqueous Na^+-based energy storage devices. Like MoO_3, the primary challenges with using V_2O_5 for aqueous energy storage are that it is a poor electron conductor and is soluble in neutral-pH aqueous solutions.[25,50–52] Efforts to improve the electronic conductivity of V_2O_5 involve the incorporation of CNTs,[96,97] graphene or reduced graphene oxide,[94] V^{4+} defects,[98] and structural water.[93,98,99] Advanced architectures with CNTs or graphene oxide ensure good electron transport to the V_2O_5,[94,96,97,100] while V^{4+} defects and structural water are reported to improve Na^+ solid state diffusion by increasing the interlayer spacing.[93,98,99] As shown by its Pourbaix diagram (**Figure 9a**), the minimum solubility of V_2O_5 is at a pH of ~ 2. Like MoO_3, V_2O_5 experiences oxidative dissolution and is stabilized during electrochemical reduction, but becomes readily soluble in neutral pH upon oxidation of vanadium to V^{5+}.[25,78]

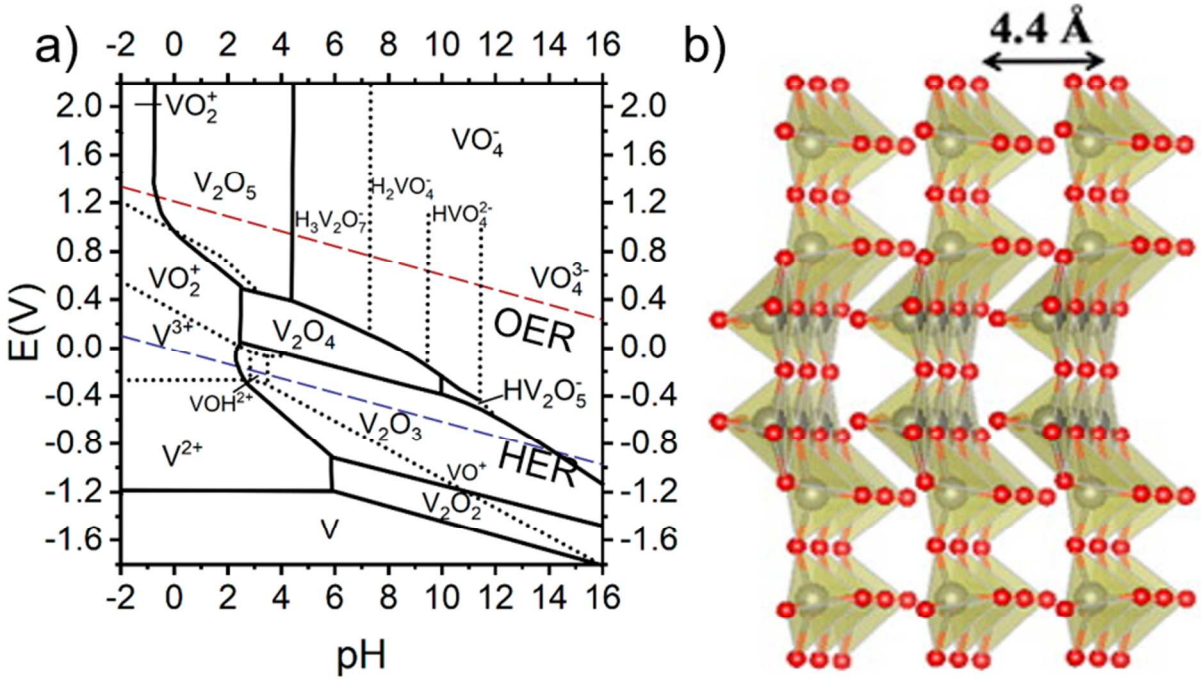

Figure 9. a) Pourbaix diagram of V_2O_5 in water (adapted from Ref. 25), b) Crystal structure of α-V_2O_5. Adapted with permission from Ref. 101. Copyright 2016 American Chemical Society.

i. α-V_2O_5

The orthorhombic (α-phase) of V_2O_5 is a layered structure with an interlayer spacing 4.4 Å; it expands and contracts along the [001] direction with Na^+ intercalation and de-intercalation (**Figure 9b**).[52] This structure is often used for aqueous electrochemical capacitor devices with Na^+ and K^+ electrolytes.[100,102] Capacities vary by morphology and synthesis technique, as shown in **Table II**. For example, crystalline, hydrothermally-synthesized nanowires showed much higher rate capability than low-temperature hydrothermally synthesized nanobelts on reduced graphene oxide.[52,94] Advanced electrode architectures, such as intertwining V_2O_5 nanobelts with CNTs (Figure 10a), have been shown to increase the capacitance from 146 F g^{-1} (73 mAh g^{-1}) to

313 F g^{-1} (157 mAh g^{-1}) while improving the intercalation kinetics, as shown in **Figure 10b**.[96] Crystalline V_2O_5 nanobelts lost 66 % of their capacity over 2,000 cycles at 10 A g^{-1}, but maintained ~ 100 % coulombic efficiency during 10,000 cycles.[52] The capacity loss was correlated with mass loss, which showed that V_2O_5 dissolved in the aqueous electrolyte. Since the capacity decline greatly slowed after ~ 2,000 cycles, it appeared that the driving force for the dissolution of V_2O_5 decreased with increased concentration of vanadates in the electrolyte.

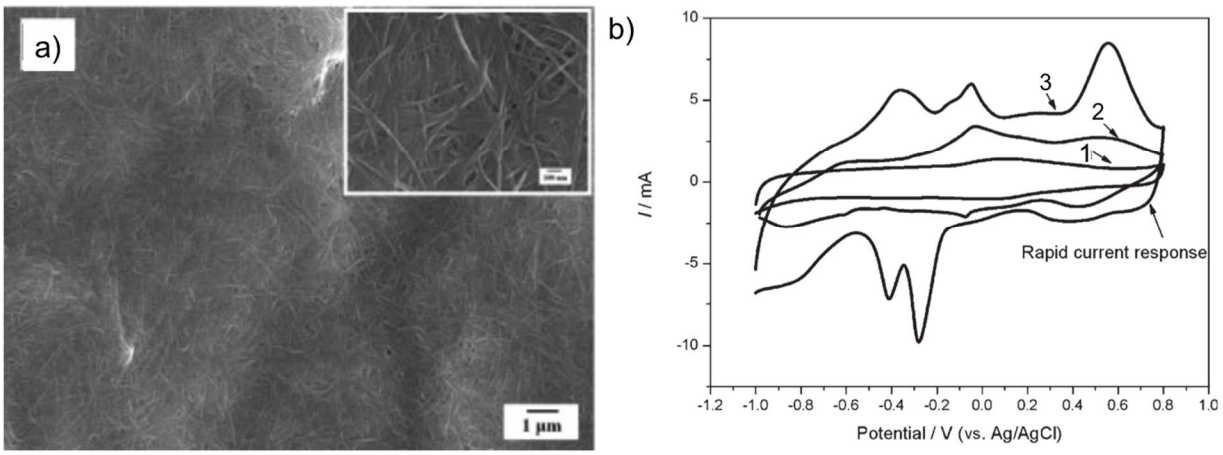

Figure 10. a) Scanning electron micrograph of the V_2O_5/CNT composite electrode, b) Cyclic voltammetry at 10 mV s^{-1} in a 1 M Na_2SO_4 aqueous electrolyte for: (1) CNTs, (2) V_2O_5 nanobelts, and (3) the V_2O_5/CNT composite. The V_2O_5/CNT composite exhibits the highest current density and most reversibility of the redox peaks, showing the advantage of *in situ* growth of oxides on CNTs. Adapted with permission from Ref. 96. Copyright 2009 John Wiley and Sons.

ii. Hydrated V_2O_5

The presence of structural water in hydrated V_2O_5 ($V_2O_5 \cdot nH_2O$) leads to large interlayer spacings, between ~ 10.6 - 12.6 Å, depending on the water content.[93,98] This can be highly beneficial in enabling high rate capability for aqueous energy storage, where cations often co-intercalate with their hydration sphere.[17] $V_2O_5 \cdot nH_2O$ can be pre-intercalated with cations, such as in $Na_2V_6O_{16} \cdot 2.6H_2O$ nanobelts, which consist of V_3O_8 layers with hydrated Na^+ ions in the interlayer.[95] The hydrated oxide can be directly synthesized by hydrothermal or sol-gel methods.[93,95] Also, like δ-MnO_2, hydrated V_2O_5 phases are capable of intercalating K^+ and Mg^{2+} in addition to Na^+ in aqueous electrolytes.[99,103,104]

Hydrated V_2O_5 does not exhibit high capacity retention; X-ray diffraction of $Na_2V_6O_{16} \cdot 2.6H_2O$ nanobelts showed that the original phase disappears after 150 cycles in aqueous Na_2SO_4 electrolyte, and that an unexplained new phase evolved with cycling.[95] This shows that unlike δ-MnO_2, hydrated V_2O_5 does not exhibit improved cycling stability over the anhydrous phase for energy storage via bulk intercalation.[35,42,43,94,95] Like MoO_3, the poor electronic conductivity and high solubility of V_2O_5 in aqueous electrolytes inhibit its performance in aqueous Na^+ energy storage. V_2O_5 may be a promising anode candidate for aqueous Na^+ energy storage in WiSE or other electrolytes that control the activity of water.

Table II. Energy storage performance of various V_2O_5 and related oxides in neutral pH aqueous Na^+ electrolytes.

Material	Capacity (mAh g^{-1})	Capacity Retention	Ref.
$Na_2V_6O_{16} \cdot 2.6H_2O$	123 (2 mV s^{-1})	34% (50 cycles at 2 mV s^{-1})	95
$Na_{1.2}V_3O_8$	55 (0.5 A g^{-1})	--	103

α-V_2O_5 nanobelt/reduced graphene oxide	64 (10 mV s^{-1})	82% (5,000 cycles at 200 mV s^{-1})	94
α-V_2O_5 nanowire	60 (2 A g^{-1})	32% (2,000 cycles at 10 A g^{-1})	52
α-V_2O_5/CNTs	220 (0.25 A g^{-1})	--	96

B. Sodium Metal Oxides

Sodium metal oxides (Na_xMO_2, where M is a transition metal) are promising cathode materials for aqueous Na^+-based energy storage devices because they undergo redox at anodic potentials and have high theoretical capacities. Since high gravimetric capacity is important for energy storage applications, most studies focus on Na_xMO_2 where M are first row transition metals such as manganese, cobalt, and/or titanium. The Na_xMO_2 crystallize into either layered or tunnel structures. The non-aqueous Na^+ intercalation electrochemistry of these materials is typically characterized by many solid state phase transformations and ordering of Na^+ and Na^+ vacancies that lead to capacity fade.[105] Significant attention has been directed toward the tunnel structures for use in aqueous energy storage devices, while research is only beginning into the electrochemical behavior of the O3 and P2 layered structures of Na_xMO_2.

In Na_xMO_2, the structure type is largely determined by the Na^+ content: tunnel structures exist for $x < 0.44$, P2 layered structures for $0.33 < x < 0.9$, and O3 layered structures for $0.9 < x < 1$.[106–109] The atmospheric stability of the structures also depends on Na^+ content, decreasing with increasing Na^+ content, so that tunnel structures are the most atmospherically stable.[109–112] The theoretical capacity of tunnel, P2, and O3 structures can be as high as ~120 mAh g^{-1}.[64,113,114] Many O3 and P2-type Na_xMO_2 are stored in an inert atmosphere immediately after synthesis to prevent degradation.[110,111] While not a perfect measure of stability, a material with an OCP below the reduction potential of water (3.94 V *vs*. Na/Na^+) will spontaneously react with water

and air.[57] For example, fully sodiated materials (x = 1) almost always have an OCP below that of the HER, and will spontaneously form an impurity phase with a lower sodium content.[67] In both the P2 and O3 layered oxides, it has been shown that some Na^+ is spontaneously removed in the presence of water, carbon dioxide, and oxygen, which oxidizes and hydrates the Na_xMO_2.[42,57,67,82,110–112,115–119]

a. Tunnel-Structured Na_xMO_2

The main advantage of the tunnel-structured $Na_{0.44}MnO_2$ (also written as $Na_4Mn_9O_{18}$) is the stability of the structure.[120] It is electrochemically active as a cathode material in aqueous Na^+ electrolytes and capable of reasonable charge storage at high rates.[4,34,64,114] The drawback of this oxide is that it experiences many phase transformations during electrochemical cycling.[4,106,114,121,122] While the theoretical capacity is ~ 120 mAh g^{-1}, only ~ 60 mAh g^{-1} is available in aqueous electrolytes as de-intercalating more Na^+ releases O_2 from the structure.[64,109,120] Due to its stability and capacity, this material has also been investigated as an electrode material for redox-based electrochemical desalination.[123]

$Na_{0.44}MnO_2$ exhibits an orthorhombic crystal structure, with 2 x 2 and 1 x 3 tunnels occupied by Na^+, Li^+, or K^+. **Figure 11a** shows the three Na and 5 Mn crystallographic sites in the structure. In the stoichiometric material (where the Na : Mn ratio is 0.44 : 1), all Na(3) sites in the 2 x 2 tunnels are filled, as well as half of the Na(1) and Na(2) sites in the 1 x 3 tunnels. The Na(1) sites are generally not electrochemically active.[120]

Early investigations of $Na_{0.44}MnO_2$ focused on its performance and rate capability in various aqueous Na^+ electrolytes.[121,124] This material was pioneered as a cathode for aqueous Na^+ batteries by Whitacre et al., who demonstrated a capacity of 45 mAh g^{-1} at 0.125 C in 1 M

Na_2SO_4 (corresponding to the storage of 0.22 Na^+ per MnO_2).[124] Its electrochemical performance, including cycling stability of a full aqueous Na^+ energy storage device, is shown in **Figure 11 b and c**. **Table III** compares the performance of $Na_{0.44}MnO_2$ with other tunnel-structured materials.

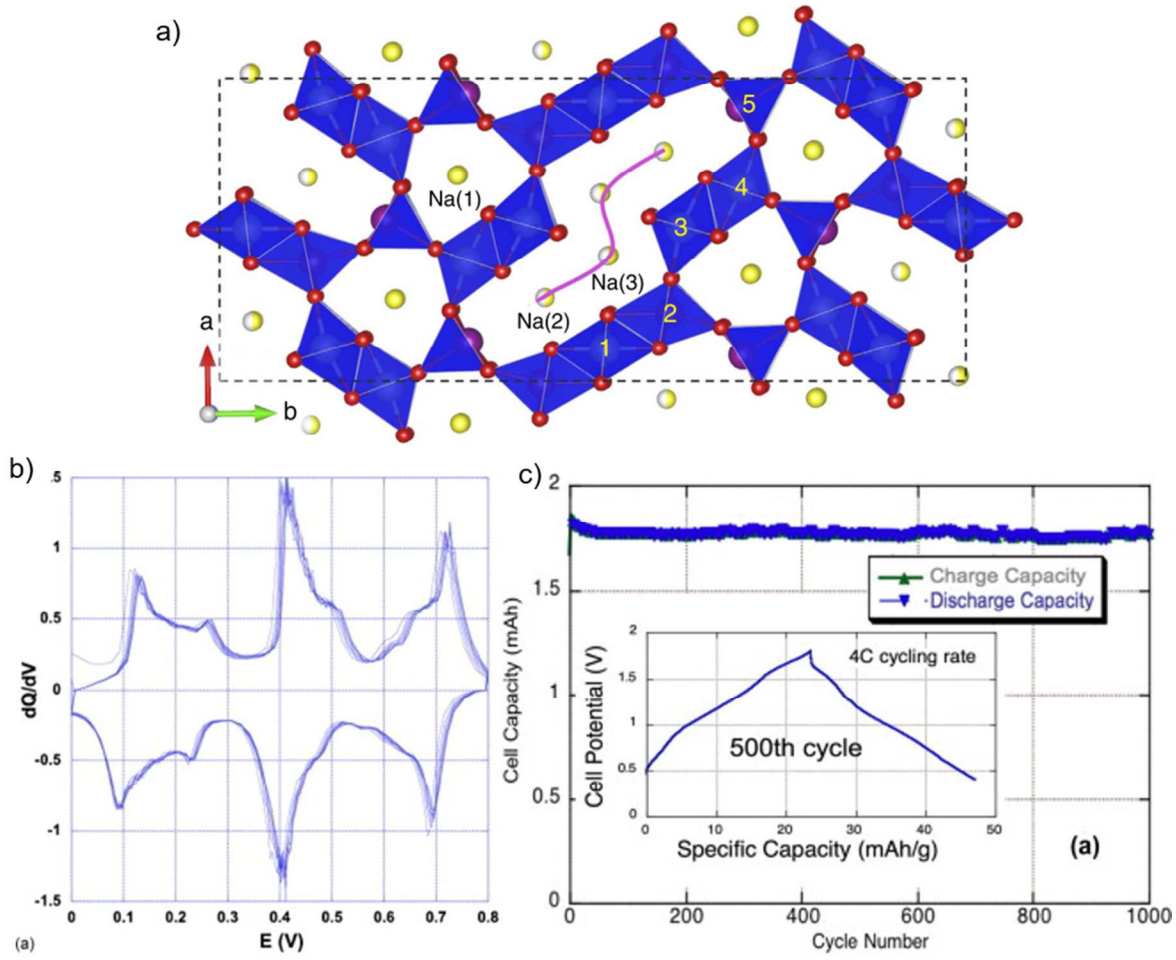

Figure 11. a) Crystal structure of tunnel-structured $Na_{0.44}MnO_2$ showing the three sodium sites and five manganese sites. Reproduced with permission from Ref. 120. Copyright 2015 Springer Nature. b) Plot of the derivative of the capacity with respect to voltage (dQ dV^{-1}) from galvanostatic cycling at 25 mA g^{-1} in a 1 M Na_2SO_4 aqueous electrolyte. Reproduced with permission from Ref. 106. Copyright 2010 The Electrochemical Society. c) Capacity retention

for 1,000 cycles at a 5C rate of a full cell with $Na_{0.44}MnO_2$ as the cathode and activated carbon as the anode. Reproduced with permission from Ref. 124. Copyright 2010 Elsevier.

The main challenge facing tunnel-structured $Na_{0.44}MnO_2$ is low capacity. Several recent studies have increased the reversible sodium content by replacing some of the manganese with transition metals that have higher redox potentials, raising the discharge potential of the oxide above 2.7 V *vs*. Na/Na^+.[64,109] Increasing the Na^+ content increases the fraction of Mn^{3+}, which decreases the tendency for irreversible O_2 evolution from the oxide lattice.[64,125–127] For example, Xu et al. added Ti and Fe to $Na_{0.44}MnO_2$ in order to increase the maximum Na^+ content to 0.61, and reported Na^+ leaving the small tunnel site for the first time in non-aqueous electrolytes.[109] In $Na_{0.44}Mn_{1-x}Ti_xO_2$, it was found that up to 0.56 Ti per formula can be substituted while maintaining a single phase.[120] The $Na_{0.44}Mn_{0.44}Ti_{0.56}O_2$ exhibited a capacity of 45 mAh g^{-1} at 2C in a Na_2SO_4 aqueous electrolyte,[64] obtaining a similar capacity to the first-reported capacity of $Na_{0.44}MnO_2$ in 1 M Na_2SO_4 but at a rate that was 16 times higher. The highest capacity reported for a tunnel-structured Na_xMO_2 material in aqueous electrolytes is 76 mAh g^{-1} at 2C, obtained with $Na_{0.66}Mn_{0.66}Ti_{0.34}O_2$.[64] This promising result shows how tuning the composition of metal oxides strongly influences the capacity.

High-angle annular dark field scanning transmission micrographs (HAADF-STEM) of $Na_{0.44}Mn_{0.44}Ti_{0.56}O_2$ clearly show the tunnels, and the corresponding STEM-electron energy loss spectrum (EELS) show that the Ti occupies the Mn(3) and Mn(4) sites in the structure (**Figure 12**).[120] Intensity peaks in the EELS region from ~ 445 – 470 eV are due to Ti, while those in the region from ~ 620 – 650 are due to Mn. The $Na_{0.44}Mn_{0.44}Ti_{0.56}O_2$ showed a smooth galvanostatic profile, which indicated that Ti substitution suppressed the many phase transformations of

$Na_{0.44}MnO_2$. The higher Mn^{2+} content in $Na_{0.44}Mn_{0.44}Ti_{0.56}O_2$ may lead to solubility issues at low rates in aqueous electrolytes. However, a subsequent study in which Na content was increased to 0.66 Na^+ ($Na_{0.66}Mn_{0.66}Ti_{0.34}O_2$) showed 89% capacity retention after 300 cycles at 2C.[64] Tunnel-structured $Na_{0.44}MnO_2$ and related oxides currently offer promising rate capability and stability as cathodes for aqueous Na^+ energy storage devices. While their capacity is smaller than those of transition metal oxide anodes, there has been significant progress recently in tuning the composition to increase capacity.

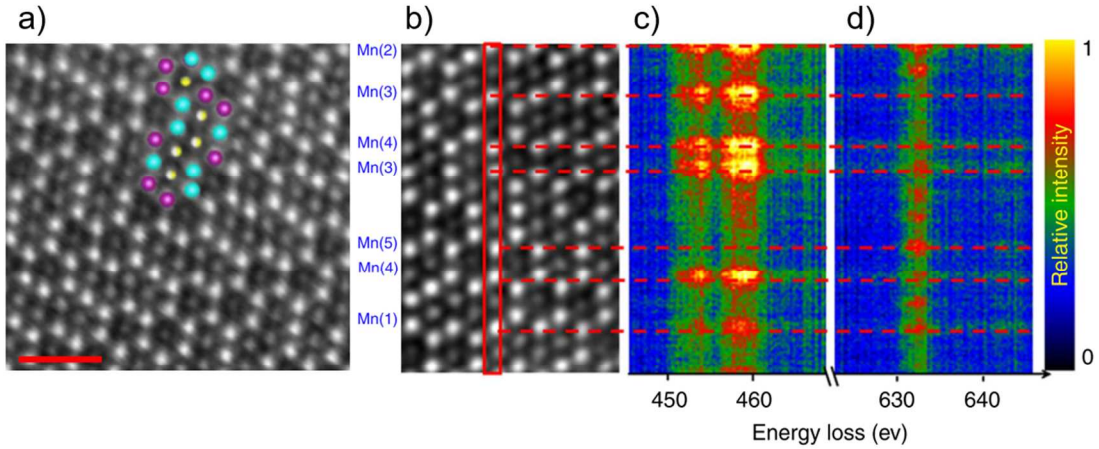

Figure 12. Occupation of Mn sites by Ti and Mn in $Na_{0.44}Mn_{0.44}Ti_{0.56}O_2$. a) & b) HAADF-STEM of the [001] zone axis, c) EELS of Ti region, and d) EELS of Mn region. These results show that Ti primarily occupies the Mn(1), (3), and (4) sites, while Mn primarily occupies the Mn(5) and Mn(2) sites. Adapted with permission from Ref. 120. Copyright 2015 Springer Nature.

Table III. Electrochemical energy storage performance of tunnel-structured Na_xMO_2.

Material	Capacity (mAh g^{-1})	Capacity Retention	Ref.
$Na_{0.44}MnO_2$	46 (0.1 A g^{-1})	90% (200 cycles, 0.2 A g^{-1})	34
$Na_{0.44}Mn_{0.44}Ti_{0.56}O_2$/NTP	45 (2 C)		64
$Na_{0.66}Mn_{0.66}Ti_{0.34}O_2$/NTP	76 (2 C)	89% (300 cycles, 2 C)	64

b. Layered P2 Na_xMO_2

P2 Na_xMO_2 consists of a layered hexagonal structure with alternating layers of Na^+ and MO_6 edge-sharing octahedra, where the Na^+ sit in trigonal prismatic sites (P). In the P2 layered structure, the "2" indicates that the oxygen layers are arranged in an …ABBA… stacking sequence along the *c*-direction (**Figure 13a**).[83] Both P2 Na_xMnO_2 and $Na_xNi_{0.22}Co_{0.11}Mn_{0.66}O_2$ rapidly form hydrated structures upon exposure to air after Na^+ de-intercalation to $x < 0.35$ Na^+.[113,116] These intercalated water molecules sit in the half-empty Na^+ sites, and counterbalance the electrostatic repulsion between MO_2 layers, mitigating the need for the layer glide experienced upon cycling in non-aqueous electrolytes.[112,113]

Thus far, there have been few reports on the aqueous electrochemistry of P2 Na_xMO_2, but their reactivity with air has received significant attention.[112,113,116,118,119,128] It has been shown that some Na^+ exchanges with H^+ upon water exposure, which may lead to Mn dissolution.[78,118,129] It has also been reported that P2 oxides with superstructure ordering of the transition metals are air and water-stable, while those without transition metal ordering transform to a hydrated structure upon exposure to air or water.[112,116] The only P2 materials reported as air or water stable to date are $Na_{0.67}Ni_{0.33}Mn_{0.67}O_2$ and $Na_{0.67}Ni_{0.33-x}Cu_xMn_{0.67}O_2$, for $0 < x < 0.33$ (both of which exhibit transition metal ordering), and $Na_{0.78}Fe_{0.22}Cu_{0.11}Mn_{0.67}O_2$.[110,112,129] While testing conditions vary, $Na_{0.6}MnO_2$, $Na_{0.67}Ni_xFe_{0.5-2x}Mn_{0.5+x}O_2$ ($0 \leq x \leq 0.15$), $Na_{0.67}Co_xNi_{0.33-x}Mn_{0.67}O_2$ ($x > 0$), $Na_{0.67}Mn_{0.8}Fe_{0.1}Ti_{0.1}O_2$, $Na_{0.63}Mn_{0.89}Zn_{0.11}O_{2.05}$, and $Na_{0.63}Mn_{0.89}Co_{0.11}O_{2.05}$ reacted upon atmospheric exposure to water, forming a hydrated phase.[111,112,116–119] Electrochemical data showed that cells made with $Na_{0.67}Ni_{0.33-x}Cu_xMn_{0.67}O_2$ ($0 < x < 0.33$) exhibited an increase in open circuit potential of ~ 0.4 V after the electrodes were exposed to air for 5 days.[110] While the reversible capacity and average voltage were not affected upon cycling in non-aqueous

electrolytes, the increase in OCP suggested that some Na^+ was removed from the oxide during exposure to air.

In one of the few studies of P2 oxides in aqueous electrolytes, Yu et al. characterized the electrochemistry of P2 $Na_{0.67}Ni_{0.25}Mn_{0.75}O_2$ in a mixed electrolyte of aqueous Na_2SO_4 and Li_2SO_4.[36] This oxide is one of the few P2 oxides that are considered air stable, and was found to be electrochemically active in the mixed aqueous electrolyte.[112] In an all-Na^+ electrolyte, the $Na_{0.67}Ni_{0.25}Mn_{0.75}O_2$ had a capacity of 41 mAh g^{-1} at 1C, with ~ 32 % capacity retention after 100 cycles at 0.1C. The capacity increased with the addition of Li_2SO_4 to the electrolyte, with the highest capacity of 62 mAh g^{-1} obtained in a 1 M Li_2SO_4 and 1 M Na_2SO_4 electrolyte with ~ 50 % capacity retention at 50 cycles at 0.1C (1C ~ 133 mA g^{-1}). While this was a reasonable capacity for an aqueous Na^+ battery, the oxide showed poor cycling performance.[31,36] P2 oxides exhibit significant degradation upon exposure to moisture, and worse electrochemical performance than δ-MnO_2.[75,87] The main mechanisms are the incorporation of water during Na^+ de-intercalation to minimize interlayer electrostatic repulsions[113,128] and the reactivity to the atmosphere of the as-synthesized materials.[111,112] Due to their reactivity with moisture and low cyclability, most P2 materials are not promising for aqueous Na^+ energy storage. However, they could show higher capacities and stability with better control of the interlayer activity and in electrolytes where the water reactivity is controlled, such as WiSE.

c. Layered O3 Na_xMO_2

The O3 structure of Na_xMO_2 is described as alternating layers of Na^+ and MO_6 octahedra. In the Delmas terminology, O3 indicates that Na^+ is in the octahedral sites (O) between layers of

MO_6 octahedra, and that the oxygens stack in an …ABC… sequence, as shown in **Figure 13b**.[83] The O3 structure can be synthesized with Na^+ content from ~ $0.65 < x < 1$.[108] Most O3 materials, including $NaMnO_2$ and $NaNi_{0.33}Mn_{0.33}Co_{0.33}O_2$, will react with the atmosphere. They experience spontaneous oxidation, interlayer hydration, formation of a Na_2CO_3 coating, and a transition from the O3 to the P3 phase.[57,67,115,127] While recent studies have reported the synthesis of O3 Na_xMO_2 that are stable upon short-term atmospheric or water exposure, the compositional factors that determine stability remain uncertain.[125,127]

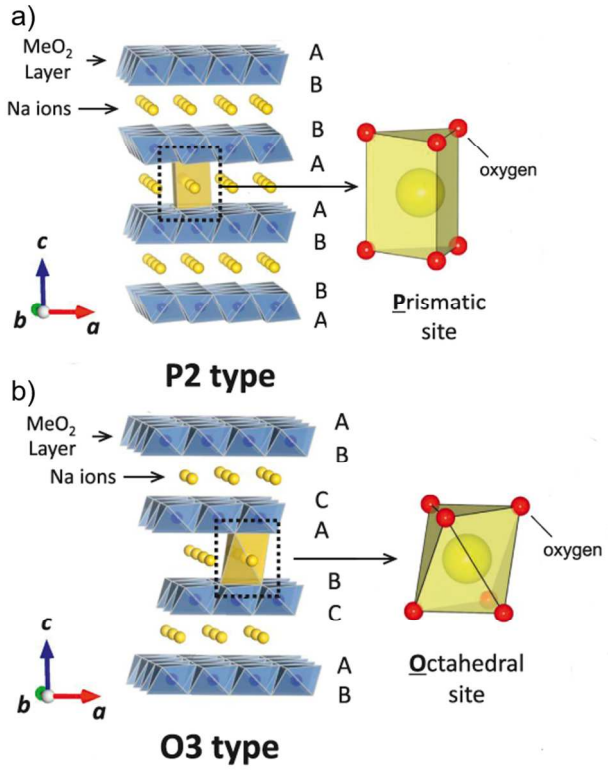

Figure 13. a) Structure of P2-Na_xMnO_2 where Na^+ occupies the prismatic interlayer sites and the oxygen stacking sequence is "…ABBA…", and b) Structure of O3 Na_xMnO_2 where Na^+

occupies the octahedral interlayer sites and the oxygen stacking sequence is "…ABC..". Adapted with permission from Ref. 130. Copyright 2014 Materials Research Society.

Thus far, the only O3 material characterized in an aqueous electrolyte is a mixed phase $NaMnO_2$.[67,115,131] Due to the inherent instability of this material, the reports of O3 $NaMnO_2$ in aqueous electrolytes characterize a mixed-phase O3-$NaMnO_2$ and P3-$Na_{0.7}MnO_2$.[67] In a full cell with activated carbon as the anode and a 0.5 M Na_2SO_4 electrolyte, this mixed-phase material exhibited a capacity of ~ 43 mAh g^{-1}, and only 3 % capacity loss after 10,000 cycles at 10C.[115] However, the capacity retention was due to the transformation of the oxide to a δ-MnO_2 -like phase after cycling. Hou et al. found that single electrodes of mixed phase O3 and P3 $NaMnO_2$ exhibited 55 mAh g^{-1} with negligible capacity loss after 500 cycles at 10C in a sodium acetate electrolyte.[67] The cycling stability was attributed to the lower solubility of manganese in sodium acetate than sodium sulfate. X-ray diffraction showed that the mixed phase O3 and P3 $NaMnO_2$ transformed to a tetragonal MnO_2 phase after 500 cycles in aqueous sodium acetate, and fracture was observed on the surface of the particles.[67] Zhang et al. characterized a cell of $Na_{0.95}MnO_2$ as the cathode and zinc metal as the anode, and found it delivered 60 mAh g^{-1} at 2C in a mixed cation electrolyte of zinc and sodium acetates (1:1 Na : Zn).[131] There was negligible capacity loss from the initial cell capacity of 40 mAh g^{-1} after 1,000 cycles at 4C, although the Coulombic efficiency only reached ~ 90 %. As with the P2 Na_xMO_2, O3 Na_xMO_2 exhibit high reactivity with the atmosphere[57,67,115,127] and this leads to structural transformations upon cycling in aqueous electrolytes. It remains to be seen whether the hydrated oxide phases formed during electrochemical cycling of O3 Na_xMO_2 exhibit better energy storage performance than transition metal oxides that exhibit minimal structural transformation in aqueous electrolytes.

IV. Future Prospects & Conclusions

Aqueous Na^+ energy storage has great potential for low-cost, highly safe energy storage applications, and increasingly, electrochemical desalination based on redox-active electrodes. The unique nature of water as an electrolyte solvent and the strong interactions between aqueous electrolytes and transition metal oxide surfaces make Na^+ intercalation processes in aqueous electrolytes distinct from those in non-aqueous electrolytes. The capacities of potential anode materials for aqueous Na^+ storage such as V_2O_5 and MoO_3 can be significant (> 150 mAh g^{-1}) while those of the cathode materials, which are primarily based on manganese-rich Na_xMO_2, are more modest (~ 70 mAh g^{-1}). Stability of the transition metal oxide is often a major concern as it limits lifetime even when high capacity is attained, and electrochemical conditions much be chosen carefully to avoid side reactions with water, including oxide dissolution. The recent WiSE strategy has promising early results and the potential to improve both the stability and energy density of aqueous Na^+ energy storage. Increased control over the water/transition metal oxide interface, including the metal oxide tunnel or interlayer regions, is likely to lead to significant improvements in performance for energy storage and desalination applications.

V. Acknowledgements

This material is based upon work supported by the National Science Foundation Graduate Research Fellowship Program under Grant No. 571800 (to S.B.).

VI. References

1 H. Kim, J. Hong, K. Y. Park, H. Kim, S. W. Kim and K. Kang, *Chem. Rev.*, 2014, **114**, 11788–11827.

2 Y. Li, Y. Lu, C. Zhao, Y.-S. Hu, M.-M. Titirici, H. Li, X. Huang and L. Chen, *Energy Storage Mater.*, 2017, **7**, 130–151.

3 M. E. Suss and V. Presser, *Joule*, 2018, **2**, 10–15.

4 W. Wu, S. Shabhag, J. Chang, A. Rutt and J. F. Whitacre, *J. Electrochem. Soc.*, 2015, **162**, A803–A808.

5 A. Bhide, J. Hofmann, A. K. Dürr, J. Janek and P. Adelhelm, *Phys. Chem. Chem. Phys.*, 2014, **16**, 1987–1998.

6 V. Augustyn, P. Simon and B. Dunn, *Energy Environ. Sci.*, 2014, **7**, 1597–1614.

7 J. C. Westall, in *Aquatic Surface Chemistry: Chemical Processes at the Particle-Water Interface*, ed. W. Stumm, John Wiley & Sons, New York, First., 1987, pp. 3–32.

8 M. A. Brown, A. Goel and Z. Abbas, *Angew. Chemie - Int. Ed.*, 2016, **55**, 3790–3794.

9 B. C. Bunker and W. H. Casey, in *The Aqueous Chemistry of Oxides*, Oxford University Press, New York, First., 2016, pp. 51–60.

10 R.-S. Kühnel, D. Reber, A. Remhof, R. Figi, D. Bleiner and C. Battaglia, *Chem. Commun.*, 2016, **52**, 10435–10438.

11 L. Athouël, F. Moser, R. Dugas, O. Crosnier, D. Bélanger and T. Brousse, *J. Phys. Chem. C*, 2008, **112**, 7270–7277.

12 J. Alvarado, C. Ma, S. Wang, K. Nguyen, M. Kodur and Y. S. Meng, *ACS Appl. Mater. Interfaces*, 2017, **9**, 26518–26530.

13 J.-Y. Hwang, S.-T. Myung and Y.-K. Sun, *Chem. Soc. Rev.*, 2017, **46**, 3529–3614.

14 L. Suo, O. Borodin, T. Gao, M. Olguin, J. Ho, X. Fan, C. Luo, C. Wang and K. Xu, *Science*, 2015, **350**, 938–943.

15 F. Wang, Y. Lin, L. Suo, X. Fan, T. Gao, C. Yang, F. Han, Y. Qi, K. Xu and C. Wang, *Energy Environ. Sci.*, 2016, **9**, 3666–3673.

16 F. Franks, in *Water: A Comprehensive Treatise. Volume 2*, ed. F. Franks, Plenum Press, New York, First., 1973, pp. 1–54.

17 M. S. Whittingham and A. J. Jacobson, Eds., *Intercalation Chemistry*, Academic Press, Inc., New York, New York, 1982.

18 B. C. Bunker and W. H. Casey, in *The Aqueous Chemistry of Oxides*, Oxford University Press, New York, First., 2016, pp. 61–86.

19 J. O. Bockris, A. K. N. Reddy and M. Gamboa-Aldeco, in *Modern Electrochemistry, Volume 1, Ionics*, Springer, New York, 2nd edn., 2002, pp. 45–174.

20 P. W. Schindler and W. Stumm, in *Aquatic Surface Chemistry: Chemical Processes at the Particle-Water Interface*, ed. W. Stumm, John Wiley & Sons, Inc., 1987, pp. 83–110.

21 B. C. Bunker and W. H. Casey, in *The Aqueous Chemistry of Oxides*, Oxford University Press, New York, First., 2016, pp. 132–157.

22 A. I. Mohamed and J. F. Whitacre, *Electrochim. Acta*, 2017, **235**, 730–739.

23 Y. Wang, J.-Y. Lou, W. Wu, C.-X. Wang and Y.-Y. Xia, *J. Electrochem. Soc.*, 2007, **154**, A228–A234.

24 K. Miyazaki, T. Shimada, S. Ito, Y. Yokoyama, T. Fukutsuka and T. Abe, *Chem. Commun.*, 2016, **52**, 4979–4982.

25 M. Pourbaix, *Atlas of electrochemical equilibria in aqueous solutions*, National Association of Corrosion Engineers, Houston, Tx, Second., 1974.

26 J.-Y. Luo, W.-J. Cui, P. He and Y.-Y. Xia, *Nat. Chem.*, 2010, **2**, 760–765.

27 Z. Hou, X. Zhang, X. Li, Y. Zhu, J. Liang and Y. Qian, *J. Mater. Chem. A*, 2017, **5**, 730–738.

28 K. Nakamoto, Y. Kano, A. Kitajou and S. Okada, *J. Power Sources*, 2016, **327**, 327–332.

29 R. Harivignesh, K. Kaliyappan, R. Thangavel, V. Aravindan, K. Kang, X. Sun, Y.-S. Lee, D. U. Kim and Y. Park, *J. Mater. Chem. A*, 2017, **5**, 8408–8415.

30 L. Suo, O. Borodin, W. Sun, X. Fan, C. Yang, F. Wang, T. Gao, Z. Ma, M. Schroeder, A. von Cresce, S. M. Russell, M. Armand, A. Angell, K. Xu and C. Wang, *Angew. Chemie - Int. Ed.*, 2016, **55**, 7136–7141.

31 L. Suo, O. Borodin, Y. Wang, X. Rong, W. Sun, X. Fan, S. Xu, M. A. Schroeder, A. V. Cresce, F. Wang, C. Yang, Y.-S. Hu, K. Xu and C. Wang, *Adv. Energy Mater.*, 2017, **7**, 1701189.

32 R.-S. Kühnel, D. Reber and C. Battaglia, *ACS Energy Lett.*, 2017, **2**, 2005–2006.

33 J. Zhao, Y. Li, X. Peng, S. Dong, J. Ma, G. Cui and L. Chen, *Electrochem. commun.*, 2016, **69**, 6–10.

34 Z. Guo, Y. Zhao, Y. Ding, X. Dong, L. Chen, J. Cao, C. Wang, Y. Xia, H. Peng and Y. Wang, *Chem*, 2017, **3**, 348–362.

35 X. Zhang, Z. Hou, X. Li, J. Liang, Y. Zhu and Y. Qian, *J. Mater. Chem. A*, 2016, **4**, 856–860.

36 F. Yu, S. Zhang, C. Fang, Y. Liu, S. He, J. Xia, J. Yang and N. Zhang, *Ceram. Int.*, 2017, **43**, 9960–9967.

37 F. Wang, X. Fan, T. Gao, W. Sun, Z. Ma, C. Yang, F. Han, K. Xu and C. Wang, *ACS Cent. Sci.*, 2017, **3**, 1121–1128.

38 J. Yin, C. Zheng, L. Qi and H. Wang, *J. Power Sources*, 2011, **196**, 4080–4087.

39 O. Borodin, L. Suo, M. Gobet, X. Ren, F. Wang, A. Faraone, J. Peng, M. Olguin, M. Schroeder, M. S. Ding, E. Gobrogge, A. von Wald Cresce, S. Munoz, J. A. Dura, S. Greenbaum, C. Wang and K. Xu, *ACS Nano*, 2017, **11**, 10462–10471.

40 J. Vatamanu and O. Borodin, *J. Phys. Chem. Lett.*, 2017, **8**, 4362–4367.

41 J. F. Whitacre, T. Wiley, S. Shanbhag, Y. Wenzhuo, A. Mohamed, S. E. Chun, E. Weber, D. Blackwood, E. Lynch-Bell, J. Gulakowski, C. Smith and D. Humphreys, *J. Power Sources*, 2012, **213**, 255–264.

42 Y. Li, X. Feng, S. Cui, Q. Shi, L. Mi and W. Chen, *CrystEngComm*, 2016, **18**, 3136–3141.

43 K. W. Nam, S. Kim, E. Yang, Y. Jung, E. Levi, D. Aurbach and J. W. Choi, *Chem. Mater.*, 2015, **27**, 3721–3725.

44 H.-S. Kim, J. B. Cook, H. Lin, J. S. Ko, S. H. Tolbert, V. Ozolins and B. Dunn, *Nat. Mater.*, 2016, **16**, 454–460.

45 Y. Li, D. Wang, Q. An, B. Ren, Y. Rong and Y. Yao, *J. Mater. Chem. A*, 2016, **4**, 5402–5405.

46 D. A. Kitchaev, S. T. Dacek, W. Sun and G. Ceder, *J. Am. Chem. Soc.*, 2017, **139**, 2672–2681.

47 M. F. Dupont and S. W. Donne, *J. Electrochem. Soc.*, 2016, **163**, A888–A897.

48 P. Ragupathy, H. N. Vasan and N. Munichandraiah, *J. Electrochem. Soc.*, 2008, **155**, A34.

49 S. Devaraj and N. Munichandraiah, *J. Phys. Chem. C*, 2008, **112**, 4406–4417.

50 M. Y. Ho, P. S. Khiew, D. Isa, W. S. Chiu and C. H. Chia, *J. Mater. Sci. Mater. Electron.*, 2017, 6907–6918.

51 P. M. Shafi, R. Dhanabal, A. Chithambararaj, S. Velmathi and A. C. Bose, *ACS Sustain. Chem. Eng.*, 2017, **5**, 4757–4770.

52 M. Yao, P. Wu, S. Cheng, L. Yang, Y. Zhu, M. Wang, H. Luo, B. Wang, D. Ye and M. Liu, *Phys. Chem. Chem. Phys.*, 2017, **19**, 24689–24695.

53 D. Chen, D. Ding, X. Li, G. H. Waller, X. Xiong, M. A. El-Sayed and M. Liu, *Chem. Mater.*, 2015, **27**, 6608–6619.

54 S. N. Lou, N. Sharma, D. Goonetilleke, W. H. Saputera, T. M. Leoni, P. Brockbank, S. Lim, D.-W. Wang, J. Scott, R. Amal and Y. H. Ng, *Adv. Energy Mater.*, 2017, **7**, 1700545.

55 Y. Liu, B. H. Zhang, S. Y. Xiao, L. L. Liu, Z. B. Wen and Y. P. Wu, *Electrochim. Acta*, 2014, **116**, 512–517.

56 X. Xiao, C. Zhang, S. Lin, L. Huang, Z. Hu, Y. Cheng, T. Li, W. Qiao, D. Long, Y. Huang, L. Mai, Y. Gogotsi and J. Zhou, *Energy Storage Mater.*, 2015, **1**, 1–8.

57 M. Sathiya, K. Hemalatha, K. Ramesha, J.-M. Tarascon and A. S. Prakash, *Chem. Mater.*, 2012, **24**, 1846−1853.

58 J. Lee, S. Kim and J. Yoon, *ACS Omega*, 2017, **2**, 1653–1659.

59 M. A. Oliver-Tolentino, J. Vazquez-Samperio, R. Cabrera-Sierra and E. Reguera, *RSC Adv.*, 2016, **6**, 108627–108634.

60 J. Liu, C. Xu, Z. Chen, S. Ni and Z. X. Shen, *Green Energy Environ.*, 2017, **1703008**, 1–31.

61 C. D. Wessells, S. V. Peddada, R. A. Huggins and Y. Cui, *Nano Lett.*, 2011, **11**, 5421–5425.

62 J. Yun, J. Pfisterer and A. S. Bandarenka, *Energy Environ. Sci.*, 2016, **9**, 955–961.

63 W. Wu, A. Mohamed and J. F. Whitacre, *J. Electrochem. Soc.*, 2013, **160**, A497–A504.

64 Y. Wang, L. Mu, J. Liu, Z. Yang, X. Yu, L. Gu, Y. S. Hu, H. Li, X. Q. Yang, L. Chen and X. Huang, *Adv. Energy Mater.*, 2015, **5**, 1501005.

65 H. Zhang, S. Jeong, B. Qin, D. Carvalho, D. Buchholz and S. Passerini, *ChemSusChem*, , DOI:10.1002/cssc.201800194.

66 W. Wu, J. Yan, A. Wise, A. Rutt and J. F. Whitacre, *J. Electrochem. Soc.*, 2014, **161**, A561–A567.

67 Z. Hou, X. Li, J. Liang, Y. Zhu and Y. Qian, *J. Mater. Chem. A*, 2015, **3**, 1400–1404.

68 W. Song, X. Ji, Y. Zhu, H. Zhu, F. Li, J. Chen, F. Lu, Y. Yao and C. E. Banks, *ChemElectroChem*, 2014, **1**, 871–876.

69 Q. Zhao, Y. Lu and J. Chen, *Adv. Energy Mater.*, 2017, **7**, 1601792.

70 S. Kim, K. W. Nam, S. Lee, W. Cho, J. S. Kim, B. G. Kim, Y. Oshima, J. S. Kim, S. G. Doo, H. Chang, D. Aurbach and J. W. Choi, *Angew. Chemie - Int. Ed.*, 2015, **54**, 15094–15099.

71 S. Kim, S. Lee, K. W. Nam, J. Shin, S. Y. Lim, W. Cho, K. Suzuki, Y. Oshima, M. Hirayama, R. Kanno and J. W. Choi, *Chem. Mater.*, 2016, **28**, 5488–5494.

72 X. F. Shen, Y. S. Ding, J. Liu, J. Cai, K. Laubernds, R. P. Zerger, A. Vasiliev, M. Aindow and S. L. Suib, *Adv. Mater.*, 2005, **17**, 805–809.

73 H. Y. Lin, Y. P. Sun, B. J. Weng, C. T. Yang, N. T. Suen, K. H. Liao, Y. C. Huang, J. Y. Ho, N. S. Chong and H. Y. Tang, *Electrochim. Acta*, 2007, **52**, 6548–6553.

74 S. W. Lee, J. Kim, S. Chen, P. T. Hammond and Y. Shao-Horn, *Am. Chem. Soc.*, 2010, **4**, 3889–3896.

75 M. Feng, Q. Du, L. Su, G. Zhang, G. Wang, Z. Ma, W. Gao, X. Qin and G. Shao, *Sci. Rep.*, 2017, **7**, 2219.

76 J. Gu, X. Fan, X. Liu, S. Li, Z. Wang, S. Tang and D. Yuan, *Chem. Eng. J.*, 2017, **324**, 35–43.

77 J. C. Hunter, *J. Solid State Chem.*, 1981, **39**, 142–147.

78 A. T. Stone and J. J. Morgan, in *Aquatic Surface Chemistry: Chemical Processes at the Particle-Water Interface*, ed. W. Stumm, John Wiley & Sons, Inc., 1987, pp. 221–254.

79 H. Y. Lee and J. B. Goodenough, *J. Solid State Chem.*, 1999, **144**, 220–223.

80 S. Komaba, N. Yabuuchi and T. Tsuchikawa, in *Electrical Phenomena at Interfaces and Biointerfaces: Fundamentals and Applications in Nano-, Bio-, and Environmental Sciences*, ed. H. Ohshima, John Wiley & Sons, Inc., First., 2012, pp. 491–507.

81 B. W. Byles, D. A. Cullen, K. L. More and E. Pomerantseva, *Nano Energy*, 2018, **44**, 476–488.

82 K. S. Abou-El-Sherbini, M. H. Askar and R. Schöllhorn, *Solid State Ionics*, 2002, **150**, 407–415.

83 C. Delmas, C. Fouassier and P. Hagenmuller, *Phys. B+C*, 1980, **99**, 81–85.

84 S. Guo, Q. Li, P. Liu, M. Chen and H. Zhou, *Nat. Commun.*, 2017, **8**, 135.

85 Y. Liu, Y. Qiao, W. Zhang, H. Wang, K. Chen, H. Zhu, Z. Li and Y. Huang, *J. Mater. Chem. A*, 2015, **3**, 7780–7785.

86 J. Shao, X. Li, Q. Qu and Y. Wu, *J. Power Sources*, 2013, **223**, 56–61.

87 Y. Liu, Y. Qiao, X. Lou, X. Zhang, W. Zhang and Y. Huang, *ACS Appl. Mater. Interfaces*, 2016, **8**, 14564–14571.

88 R. Schöllhorn, R. Kuhlmann and J. O. Besenhard, *Mater. Res. Bull.*, 1976, **11**, 83–90.

89 K. Inzani, M. Nematollahi, F. Vullum-Bruer, T. Grande, T. W. Reenaas and S. M. Selbach, *Phys. Chem. Chem. Phys.*, 2017, **19**, 9232–9245.

90 T. Li, M. Beidaghi, X. Xiao, L. Huang, Z. Hu, W. Sun, X. Chen, Y. Gogotsi and J. Zhou, *Nano Energy*, 2016, **26**, 100–107.

91 L. Huang, B. Yao, J. Sun, X. Gao, J. Wu, J. Wan, T. Li, Z. Hu and J. Zhou, *J. Mater. Chem. A*, 2017, **5**, 2897–2903.

92 I. A. de Castro, R. S. Datta, J. Z. Ou, A. Castellanos-Gomez, S. Sriram, T. Daeneke and K. Kalantar-zadeh, *Adv. Mater.*, 2017, **29**, 1–31.

93 Q. Wei, J. Liu, W. Feng, J. Sheng, X. Tian, L. He, Q. An and L. Mai, *J. Mater. Chem. A*, 2015, **3**, 8070–8075.

94 M. Lee, S. K. Balasingam, H. Y. Jeong, W. G. Hong, H.-B.-R. Lee, B. H. Kim and Y. Jun, *Sci. Rep.*, 2015, **5**, 8151.

95 C. Deng, S. Zhang, Z. Dong and Y. Shang, *Nano Energy*, 2014, **4**, 49–55.

96 Z. Chen, Y. Qin, D. Weng, Q. Xiao, Y. Peng, X. Wang, H. Li, F. Wei and Y. Lu, *Adv. Funct. Mater.*, 2009, **19**, 3420–3426.

97 J. Wu, X. Gao, H. Yu, T. Ding, Y. Yan, B. Yao, X. Yao, D. Chen, M. Liu and L. Huang, *Adv. Funct. Mater.*, 2016, **26**, 6114–6120.

98 S. Li, X. Li, Y. Li, B. Yan, X. Song, L. Fan, H. Shan and D. Li, *J. Alloys Compd.*, 2017, **722**, 278–286.

99 D. S. Charles, M. Feygenson, K. Page, J. Neuefeind, W. Xu and X. Teng, *Nat. Commun.*, 2017, **8**, 15520.

100 A. Choudhury, J. H. Kim, K. S. Yang and D. J. Yang, *Electrochim. Acta*, 2016, **213**, 400–407.

101 G. Ali, J. H. Lee, S. H. Oh, B. W. Cho, K. W. Nam and K. Y. Chung, *ACS Appl. Mater. Interfaces*, 2016, **8**, 6032–6039.

102 R. S. Ingole and B. J. Lokhande, *J. Mater. Sci. Mater. Electron.*, 2017, **28**, 10951–10957.

103 M. Vujković, B. S. Paunković, I. S. Simatović, M. Mitrić, C. A. C. Sequeira and S. Mentus, *Electrochim. Acta*, 2014, **147**, 167–175.

104 R. S. Ingole and B. J. Lokhande, *J. Mater. Sci. Mater. Electron.*, 2017, **28**, 10951–10957.

105 R. Berthelot, D. Carlier and C. Delmas, *Nat. Mater.*, 2011, **10**, 74–80.

106 A. D. Tevar and J. F. Whitacre, *J. Electrochem. Soc.*, 2010, **157**, A870–A875.

107 B. Mortemard de Boisse, D. Carlier, M. Guignard and C. Delmas, *J. Electrochem. Soc.*, 2013, **160**, A569–A574.

108 J. S. Thorne, R. A. Dunlap and M. N. Obrovac, *J. Electrochem. Soc.*, 2012, **160**, A361–A367.

109 S. Xu, Y. Wang, L. Ben, Y. Lyu, N. Song, Z. Yang, Y. Li, L. Mu, H. T. Yang, L. Gu, Y. S. Hu, H. Li, Z. H. Cheng, L. Chen and X. Huang, *Adv. Energy Mater.*, 2015, **5**, 1–9.

110 L. Zheng, J. Li and M. N. Obrovac, *Chem. Mater.*, 2017, **29**, 1623–1631.

111 V. Duffort, E. Talaie, R. Black and L. F. Nazar, *Chem. Mater.*, 2015, **27**, 2515–2524.

112 Z. Lu and J. R. Dahn, *Chem. Mater.*, 2001, **13**, 1252–1257.

113 D. Buchholz, L. G. Chagas, C. Vaalma, L. Wu and S. Passerini, *J. Mater. Chem. A*, 2014, **2**, 13415–13421.

114 Z. Li, D. Young, K. Xiang, W. C. Carter and Y. Chiang, *Adv. Energy Mater.*, 2013, **3**, 290–294.

115 Q. T. Qu, Y. Shi, S. Tian, Y. H. Chen, Y. P. Wu and R. Holze, *J. Power Sources*, 2009,

194, 1222–1225.

116 A. Caballero, L. Hernán, J. Morales, L. Sánchez, J. Santos Peña and M. A. G. Aranda, *J. Mater. Chem.*, 2002, **12**, 1142–1147.

117 T. A. Eriksson, Y. J. Lee, J. Hollingsworth, J. A. Reimer, E. J. Cairns, X. F. Zhang and M. M. Doeff, *Chem. Mater.*, 2003, **15**, 4456–4463.

118 M. H. Han, N. Sharma, E. Gonzalo, J. C. Pramudita, H. E. A. Brand, J. M. López del Amo and T. Rojo, *J. Mater. Chem. A*, 2016, **4**, 18963–18975.

119 M. H. Han, E. Gonzalo, N. Sharma, J. M. López Del Amo, M. Armand, M. Avdeev, J. J. Saiz Garitaonandia and T. Rojo, *Chem. Mater.*, 2016, **28**, 106–116.

120 Y. Wang, J. Liu, B. Lee, R. Qiao, Z. Yang, S. Xu, X. Yu, L. Gu, Y. Hu, W. Yang, K. Kang, H. Li, X. Yang, L. Chen and X. Huang, *Nat. Commun.*, 2015, **6**, 1–10.

121 F. Sauvage, E. Baudrin and J. M. Tarascon, *Sensors Actuators, B Chem.*, 2007, **120**, 638–644.

122 G. Pang, P. Nie, C. Yuan, L. Shen, X. Zhang, J. Zhu and B. Ding, *Energy Technol.*, 2014, **2**, 705–712.

123 F. Chen, Y. Huang, L. Guo, M. Ding and H. Y. Yang, *Nanoscale*, 2017, **9**, 10101–10108.

124 J. F. Whitacre, A. Tevar and S. Sharma, *Electrochem. commun.*, 2010, **12**, 463–466.

125 H. Yao, P. Wang, Y. Gong, J. Zhang, X. Yu, L. Gu, Y. Yin, E. Hu, X. Yang, E. Stavitski, Y. Guo, L. Wan, H. Yao, P. Wang, Y. Gong, J. Zhang, X. Yu, L. Gu, C. Ouyang, Y. Yin, E. Hu, X. Yang, E. Stavitski, Y. Guo and L. Wan, *J. Am. Chem. Soc.*, 2017, **139**, 8440–8443.

126 J. Deng, W.-B. Luo, X. Lu, Q. Yao, Z. Wang, H.-K. Liu, H. Zhou and S.-X. Dou, *Adv. Energy Mater.*, 2017, **1701610**, 1701610.

127 L. Mu, S. Xu, Y. Li, Y. S. Hu, H. Li, L. Chen and X. Huang, *Adv. Mater.*, 2015, **27**, 6928–6933.

128 Y. Li, Z. Yang, S. Xu, L. Mu, L. Gu, Y. Hu, H. Li and L. Chen, *Adv. Sci.*, 2015, **2**, 1500031.

129 D. Buchholz, A. Moretti, R. Kloepsch, S. Nowak, V. Siozios, M. Winter and S. Passerini, *Chem. Mater.*, 2013, **25**, 142–148.

130 K. Kubota, N. Yabuuchi, H. Yoshida, M. Dahbi and S. Komaba, *MRS Bull.*, 2014, **39**, 416–422.

131 B. Zhang, Y. Liu, X. Wu, Y. Yang, Z. Chang, Z. Wen and Y. Wu, *Chem. Commun.*, 2014, **50**, 1209–1211.